The activation mechanisms of ANO6/TMEM16F Ca^{2+}-activated chloride channel

칼슘의존성 염소이온통로 ANO6 의 활성화 기전

2019 년 02 월

서울대학교 의과대학

의학과 의학전공

림해월

A Thesis of the Degree of Doctor of Philosophy

칼슘의존성 염소이온통로

ANO6 의 활성화 기전

The activation mechanisms of

ANO6/TMEM16F Ca^{2+} −

activated chloride channel

February 2019

The Department of Medicine,

Seoul National University

College of Medicine

Haiyue Lin

칼슘의존성 염소이온통로 ANO6의 활성화 기전

지도교수 김성준
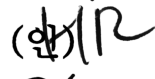
이 논문을 의학박사 학위논문으로 제출함

2018 년 10 월

서울대학교 의과대학
의학과 의학전공
림해월

림해월의 의학박사 학위논문을 인준함

2018 년 12 월

위 원 장 　　서 인석　　 (인)

부위원장 　　김 성준　　 (인)

위　 원 　　예 상규　　 (인)

위　 원 　　김 형래　　 (인)

위　 원 　　강 동묵　　 (인)
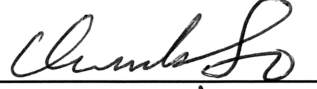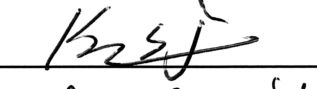
The activation mechanisms of ANO6/TMEM16F Ca^{2+} – activated chloride channel

by

Haiyue Lin

A thesis submitted to the Department of medicine
in partial fulfillment of the requirements for the
Degree of Doctor of Philosophy in Medicine at
Seoul National University College of Medicine

December 2018

Approved by Thesis Committee:

Professor _____ Chairman

Professor _____ Vice chairman

Professor _____

Professor _____

Professor _____

ABSTRACT

Anoctamin 6 (ANO6/TMEM16F) is a membrane protein having dual functions; calcium-activated chloride channel (CaCC) and phospholipid scramblase. Unlike other CaCCs, the activation of ANO6 requires pathological high Ca^{2+} in the cytosol ($[Ca^{2+}]_i >$ several μM) with very slow kinetics, and there has been controversy over the physiological implication of ANO6 as CaCC. Here I propose to hypotheses on the slow kinetics of ANO6 activation; 1) inhibitory influence of actin filament cytoskeleton that requires ATP, 2) putative temperature dependence of ANO6. Whole-cell patch clamp recording of ANO6 current (I_{ANO6}) was conducted with ANO6 variant 1 (V1) overexpressed HEK293T cells. In comparison with ATP-free pipette solution containing 10 μM $[Ca^{2+}]_i$, the inclusion of 3 mM ATP dramatically slowed the activation of I_{ANO6}. Also, disruption of the actin cytoskeleton with cytochalasin-D (cytoD) significantly accelerated the activation of I_{ANO6} even with ATP, while the actin filament stabilizers (phalloidin and jasplakinolide) inhibited I_{ANO6}. The excision of membrane patch, i.e. inside-out recording mode, I_{ANO6} showed immediate activation when exposed to 10 μM $[Ca^{2+}]_i$. These results suggest that the robustness of actin cytoskeleton might hamper the Ca^{2+}-dependent activation of I_{ANO6}.

  To investigate the influence of temperature, I examined the three types of ANO6 splicing variants (V1, V2 and V5; V3 did not show

plasma membrane expression). I_{ANO6} of V1, V2 and V5 commonly showed low Ca^{2+}-sensitivity and highly delayed activation in room temperature. Interestingly, at physiological temperature (37℃), the Ca^{2+} sensitivity of I_{ANO6} was largely increased even with 1 mM ATP; started to be activated by 1 μM (V1) or by 300 nM $[Ca^{2+}]_i$ (V2 and V5). Further increase of temperature to 42℃ revealed the I_{ANO6} activation by 100 nM $[Ca^{2+}]_i$ in all the three variants. The activation kinetics was also accelerated by the temperature increase; the delay time for full activation of I_{ANO6} was significantly shortened at 37℃. Notably, the temperature-dependent Ca^{2+}-sensitization of ANO6 became insignificant under inside-out patch clamp condition. Unlike the channel activity, physiological temperature did not induce the scramblase function of ANO6 with submicromolar $[Ca^{2+}]_i$ (300 nM), irrespective of variant types.

Taken together, the results offered negative cytosolic modulators actin cytoskeleton and ATP for I_{ANO6}, and suggested that all functional isoforms of ANO6 can be activated by physiological ranges of temperature. This study revealed the physiologically meaningful anion conducting property of ANO6 might precede the scramblase activity.

Anoctamin 6; TMEM16F; Calcium activated chloride channel; Actin cytoskeleton; ATP; Splicing variants; Temperature; Activation kinetics; Calcium sensitivity; Scramblase

CONTENTS

LIST OF TABLES AND FIGURES

Part 1

Part 2

LIST OF ABBREVIATIONS

ACA: N-(p-Amylcinnamoyl) anthranilic acid

ANO: Anoctamin

CaCC: Calcium activated chloride channel

CytoD: Cytochalasin-D

$[Ca^{2+}]_i$: Intracellular calcium concentration

DAPI: 4',6-diamidino-2-phenyliodole

FACS: Fluorescence-activated cell sorting

ICC: Immunocytochemistry

MAFP: Methyl arachidonyl fluorophosphonate

NEM: N-ethylmaleimide

NMDG-Cl: N-methyl-d-glucamine-Cl

NT: Normal tyroid

PI: Propidium iodide

PIP2: Phosphatidylinositol-(4,5)-bisphosphate

PLA2: Phospholipase A2

PS: Phosphatidylserine

RT: Room temperature

SSRI: Serotonin-specific reuptake inhibitor

t_{peak}: Time to peak current

GENERAL INTRODUCTION

The TMEM16 family of proteins, also known as anoctamins (ANOs), comprise several members that function as calcium (Ca^{2+})-activated chloride channels (CaCCs)[1]. The most well-known CaCCs in this group, TMEM16A (ANO1) and TMEM16B (ANO2), play fundamental roles in various physiological processes. ANO1 mediates transepithelial secretions in several gland tissues, possesses pacemaker potential for gastrointestinal motility, and acts as a heat sensor in nociception[2-6], whereas ANO2 is believed to be associated with olfactory sensory transduction and photoreceptor signalling[7,8].

 In contrast, ANO6 (TMEM16F) has dual functions which acts as a phospholipid scramblase as well as a CaCC. As a scramblase, ANO6 plays essential roles in platelet coagulant activity, induces pro-apoptotic signals in lymphocytes, induces phagocytosis as a downstream target of P2X7 receptors in macrophages, deposits hydroxyapatite in osteoblasts, and restricts T cell responses to maintain the balance of the immune reaction[9-16]. Clinically, ANO6 has been found to be mutated in patients with Scott syndrome who have impaired blood coagulation due to phospholipid scrambling defect[17,18]. As an ion channel, ANO6 shows voltage-dependent activity and has been suggested to be a component of the outwardly rectifying chloride channel[19,20], even though there is a suggestion that it is a Ca^{2+}-activated cation channel[21]. Despite the controversy

of ionic selectivity, ANO6 is generally regarded as a Ca^{2+}-activated chloride channel[11,22-25].

However, the role of ANO6 as a physiologically meaningful ion channel remains controversial. The debate largely stems from the fact that ANO6 activation requires a very high intracellular Ca^{2+} concentration ($[Ca^{2+}]_i$). The reported half-maximal Ca^{2+} concentrations (EC_{50}) for ANO6 are quite variable, ranging from several μM to 0.1 mM[22-24]. Furthermore, even with a high $[Ca^{2+}]_i$, appearance of the ANO6 current is generally delayed and requires several minutes for full activation. These properties are largely different from those of the ANO1 current that is activated with a submicromolar EC_{50} (400 nM) of $[Ca^{2+}]_i$, showing no delayed activation in response to Ca^{2+} signals[26,27].

Taken together, the previous whole-cell patch clamp studies have revealed several distinct properties of I_{ANO6} showed; 1) voltage-dependent strong outwardly rectifying current, 2) very low Ca^{2+} sensitivity (> several μM of $[Ca^{2+}]_i$ for activation), and 3) very slow activation; more than 3-5 min to reach peak level after membrane break-in, 4) poor ion selectivity (even permeable to cations)[22-25,28]. The present study focused on the low Ca^{2+} sensitivity and slow kinetics of ANO6. The role of actin cytoskeleton (Part 1) and temperature condition (Part 2) were proposed as the regulatory factors of ANO6.

MATERIALS AND METHODS

Cell culture

HEK293T cells (American Type Culture Collection, Manassas, VA, USA) were grown in high-glucose Dulbecco's modified Eagle's medium (Thermo Fisher Scientific, Waltham, MA, USA) supplemented with 10% fetal bovine serum (Thermo Fisher Scientific) at 37°C, 5 % CO_2 humidified incubator. HEK293T cells were cultured on 12-well plate, 35-mm dishes or 75-T flasks for ICC, electrophysiology, calcium measurements, and flow cytometric analysis, respectively.

Plasmids and transfection

The mammalian expression plasmid used for expressing V1 human ANO6 (hANO6) splicing variant and the human ANO1-pEGFP (ac isoform) were described previously[24]. The cDNAs of V2, V3, and V5 hANO6 splicing variants were purchased from GeneCopoeia™ (Rockville, MD, USA). The coding regions of hANO6 V1 (GenBank accession no. NM_001025356.2), V2 (NM_001142678.1), V3 (NM_001142679.1), and V5 (NM_001204803.1) were subcloned into the mammalian expression vector pcDNA 3.1(+) (Thermo Fisher Scientific) with a Kozak consensus sequence (GCCACC) immediately upstream of the initiation codon using polymerase chain reaction amplification. The plasmids were transiently

transfected to HEK293T cells using Turbofect transfection reagent (Thermo Fisher Scientific) according to manufacturer instructions. For electrophysiological experiments, HEK293T cells (cultured in 35-mm dishes) were co-transfected with 0.9 μg of the hANO6 variant plasmids along with 0.1 μg of the green fluorescent protein (GFP) expression plasmid to visualize the transfected cells and 1 μg of hANO1-pEGFP plasmid was transfected into HEK293T cells for whole-cell patch clamp. For ICC, cells were transfected with 1 μg of hANO6 V1 plasmid. For western blotting, calcium measurements, and FACS analysis, HEK293T cells (grown in 75-T flasks) were transfected with 4.5 μg of each ANO6 variant plasmid. Experiments were performed within 24-36 h after transfection.

Chemicals

All chemicals used for making solutions of electrophysiology were purchased from Sigma-Aldrich. The drugs cytochalasin D (cytoD), fluoxetine, and ionomycin were also purchased from Sigma-Aldrich, and jasplakinolide was from Santa-Cruz (Santa Cruz, CA, USA).

Electrophysiology

Whole-cell and inside-out patch clamp techniques were applied for measuring the channel activities of ANO6 variant-transfected

4

HEK293T cells. Cells were transferred to a bath mounted on the stage of an IX-50 inverted microscope (Olympus, Osaka, Japan) equipped with a light source set to green fluorescence excitation wavelengths. The patch-clamp experiment was performed at RT or 27°C or 37°C. The temperature was maintained by a circulating water bath and was continuously measured in a bath chamber to be maintained at exactly 27°C and 37°C (KeumSung Scientific, Seoul, Korea). Microglass pipettes (World Precision Instruments, Sarasota, FL, USA) were fabricated using a PP-830 single-stage glass microelectrode puller (Narishige, Tokyo, Japan), and with a resistance of 2.5–3.5 MΩ and 5–6 MΩ for whole-cell and inside-out patch recordings, respectively, using an MF-830 microforge (Narishige, Tokyo, Japan). Currents were recorded using an Axopatch 200B amplifier and Digidata1440A interface, digitized at 10 kHz and low pass-filtered at 5 kHz by pClamp software 10.7 (Molecular Devices, Sunnyvale, CA, USA). The series resistance and junction potential were compensated by an offset circuit in Axopatch 200B. All voltage and current trace data were analyzed by using Clampfit 10.7 and Origin 8.0 software (Microcal, Northampton, MA, USA). The detailed stimulation voltage protocols are described in the relevant figure legends.

Solutions

The whole-cell patch clamp analysis of ANO6 for both parts was conducted using a basal extracellular solution containing 146 mM N-methyl-d-glucamine-Cl (NMDG-Cl), 1 mM $CaCl_2$, 1 mM $MgCl_2$, 10 mM HEPES, and 10 mM glucose (adjusted to pH 7.4 with NMDG-OH).

For part 1, unless otherwise mentioned, the basal pipette solution (ATP-free) contained 136 mM NMDG-Cl, 10 mM HEDTA, and 5 mM HEPES, and 7.2 mM $CaCl_2$ was added to the pipette solution to obtain a free Ca^{2+} concentration of 10 μM (adjusted to pH 7.2 with NMDG-OH). The pipette solution contained 3 mM MgATP or 3 mM Na_2ATP, and 6.2 mM or 7.7 mM $CaCl_2$ were added, respectively, to obtain 10 μM free Ca^{2+} concentration. WEBMAX-C software (C. Patton, Stanford University, ww.stanford.edu/~cpatton/maxc.html) was used to calculate the accurate amount of $CaCl_2$ for 10 μM free Ca^{2+} concentration. Given that two Cl^- ions bind to one Ca^{2+} ion, appropriate amounts of NMDG-Cl were added to the basal pipette solution to adjust the Cl^- concentration to 150 mM. For the inside-out patch clamp experiment, the external solution (pH 7.4) of the whole-cell patch clamp was used as the pipette solution and the basal pipette solution (ATP-free, 10 μM free Ca^{2+}, pH 7.2) was used as the bath solution.

For part 2, the basal pipette solution contained 10 mM EGTA, 5 mM HEPES, 0.5 mM $MgCl_2$, and 1 mM Mg-ATP; an appropriate

amount of $CaCl_2$ was added to the pipette solution to obtain a Ca^{2+} concentration of 0.1, 0.3, 1, 3, and 100 μM for the 27°C, 37°C and 42°C experimental condition (adjusted to pH 7.2 with NMDG-OH). WEBMAX-C software (C. Patton, Stanford University, ww.stanford.edu/~cpatton/maxc.html) was used to calculate the accurate amount of $CaCl_2$ for each free Ca^{2+} concentration at 27°C, 37°C and 42°C. Because Ca^{2+} chelation by EGTA is weak when the free Ca^{2+} concentration is 100 μM, 10 mM HEDTA was used. Given that two Cl^- ions bind to one Ca^{2+} ion, appropriate amounts of NMDG-Cl were added to the basal pipette solution to adjust the Cl^- concentration to 150 mM. For the inside-out patch clamp experiment, the basal pipette solution contained 150 mM NMDG-Cl, 1 mM EGTA, and 5 mM HEPES (pH 7.4). The bath solution for the intracellular side of the patch contained150 mM NMDG-Cl, 1 mM EGTA, and 5 mM HEPES (pH 7.2). To obtain different concentrations of free Ca^{2+}, 10 mM EGTA or HEDTA was added to the bath solution, and an appropriate amount of $CaCl_2$ was added to change the free Ca^{2+} concentration as described above.

Immunocytochemistry

ANO6 variant 1-expressing HEK293T cells were grown on 18-mm cover slips in 12-well plates and treated with 30 μM cytoD for 1 h, with 10 μM ionomycin and 30 μM fluoxetine for 15 min at 37°C. The treated cells were washed with PBS and fixed with 4 %

paraformaldehyde for 30 min at RT. After a brief wash with PBS, the cells were permeabilized with 0.1 % Triton X-100 for 15 min. Then, the cells were incubated with 1:200 diluted phalloidin-FITC (Sigma-Aldrich, St. Louis, MO, USA) for 40 min at RT and with 1:10000 diluted DAPI (Sigma-Aldrich) for 30 s. Finally, the cover slips were mounted on glass slides with mounting medium (Invitrogen, Carlsbad, CA, USA). Images were acquired with a ZEISS LSM700 confocal microscope with a 63× oil immersion objective.

Cell surface biotinylation and immunoblotting assay

Surface biotinylation and immunoblotting were performed using conventional methods as described previously[29,30]. In brief, transfected HEK293T cells were washed three times with ice-cold phosphate-buffered saline (PBS). The cells were then treated with sulpho-NHS-SS-biotin (Pierce, Rockford, IL, USA) containing buffer for 30 min at 4°C to biotinylate the plasma membrane proteins. After biotinylation, the cells were washed with quenching buffer to remove the excess biotin and washed twice again with PBS. The cells were harvested and incubated overnight with avidin solution (Ultra-Link Immobilized NeutrAvidin Beads 10%, Pierce) at 4°C. Avidin-bound complexes were washed three times and the biotinylated proteins were eluted in a 2× sample buffer. The protein samples were suspended in a

sodium dodecylsulphate (SDS) buffer and separated by SDS-polyacrylamide gel electrophoresis. The separated proteins were transferred to a nitrocellulose membrane and blotted with appropriate primary and secondary antibodies. Anti-ANO6 (G-14; Santa Cruz Biotechnology, Santa Cruz, CA, USA) antibody was used as the primary antibody, and horseradish peroxidase-conjugated anti-rabbit IgG (Thermo Fisher Scientific) was used as the secondary antibody. Protein bands were detected by enhanced chemiluminescence (Amersham Biosciences, Buckinghamshire, UK).

Intracellular calcium measurement

$[Ca^{2+}]_i$ was measured using the fluorescent Ca^{2+} indicator Fura-2 acetoxymethyl ester (Fura-2 AM; Thermo Fisher Scientific). HEK293T cells were transiently transfected with hANO6 variants (V1, V2, and V5), and then incubated with normal tyrode (NT) solution (145 mM NaCl, 10 mM HEPES, 5 mM glucose, 3.6 mM KCl, 1.5 mM $CaCl_2$, and 1 mM $MgCl_2$; pH 7.4 adjusted with NaOH) containing 2 μM Fura-2 AM for 30 min at 37°C and washed twice with NT. Fluorescence was monitored in a quartz microcuvette (1 mL) with stirring in a temperature-controlled (37°C) cell holder of a fluorescence spectrophotometer (Photon Technology International, Birmingham, NJ, USA) at excitation wavelengths of 340 nm and 380 nm, and an emission wavelength of 510 nm. At

the end of each experiment, 5 μM ionomycin was applied to produce the maximum fluorescence ratio (R_{max}: 340/380 nm). Subsequently, 20 mM EGTA was added to confirm the minimum fluorescence ratio (R_{min}: 340/380 nm). The $[Ca^{2+}]_i$ values were calculated using the equation $[Ca^{2+}]_i = K_d \times b \times (R - R_{min})/(R_{max} - R)$, where K_d is the dissociation constant (224 nM) of Fura-2 AM and b is the ratio of the fluorescence excitation intensities of Fura-2 AM at 380 nm under Ca^{2+}-free and Ca^{2+}-saturated conditions.

Flow cytometry

hANO6 variants-transfected HEK293T cells were incubated with the appropriate concentration of ionomycin that resulted in a fixed $[Ca^{2+}]_i$ for 15 min or 30 min at 37°C. The cells were then resuspended with 100 μL Annexin V binding buffer (2.5 μL Annexin V-488 and 1 μg·mL^{-1} propidium iodide (PI); (Invitrogen, Carlsbad, CA, USA) in 5-mL polystyrene round-bottom tubes. The tubes were then gently vortexed and incubated in the dark for 15 min at 4°C, and 400 μL of the binding buffer was added to each tube before flow cytometry analysis using the FACSCalibur system (BD Bioscience, San Jose, CA, USA). To avoid the influence of ionomycin on the cells, the treated cells were maintained at 4°C for all processes until the flow cytometric analysis.

Statistical analysis

The results are expressed as the means ± standard error of mean (SEM). Statistical analysis was performed by one-way analysis of variance (ANOVA) with Tukey's HSD post-hoc tests and two-way ANOVA with Bonferroni post-hoc test for multiple comparisons. $P < 0.05$ was considered statistically significant.

PART 1. Inhibitory regulation of ANO6 by actin cytoskeleton with ATP

Introduction

This part of study focused on the unique delayed activation property of ANO6, the feature neither ANO1 nor ANO2 possesses[31,32]. According to previous studies, patch-clamp configuration affects the activation kinetics of ANO6, that inside-out patch clamp recordings show a nearly immediate activation of ANO6 in response to an increase $[Ca^{2+}]_i$ whereas the whole-cell patch clamp recordings show delayed activation[24,33]. Such results suggest that there may be unknown cytosolic factor(s) or structural cell components play roles for the determination of ANO6 activation kinetics. In this study, I examined the cytoskeleton and intracellular ATP, which can be definitely altered by changing the patch-clamp configuration.

Among the cytoskeletal proteins, the actin cytoskeleton regulates ion channels[34]. And actin depolymerization modified the channel kinetics of ANO1, another member of the TMEM16 family[35]. However, about the role of actin cytoskeleton on ANO6 activity, particularly on delayed channel activation, has not been investigated before.

Additionally, intracellular ATP can regulate diverse ion channels through direct or indirect mechanisms[33,36,37]. In the context of present study, intracellular ATP is associated with actin filament homeostasis because actin polymerization requires ATP. So, the experimental comparison of ANO6 activation in the presence and absence of ATP together with actin cytoskeleton alteration by disrupter or stabilizer might provide new insights into the regulatory mechanisms of ANO6, even though further investigations are need for the interpretations. In addition to the slow activation to peak currents, spontaneous decay of whole-cell I_{ANO6}(inactivation) has been observed[24]. Thus, I also compared the effects of actin-depolymerizing agents and ATP on the extent of ANO6 inactivation.

Results

Slow kinetics of ANO6 activation in whole-cell patch clamp

With symmetrical NMDG-Cl solutions, the $[Ca^{2+}]_i$ was clamped at 10 μM without MgATP. The whole-cell recordings were performed in ANO6 V1-overexpressed HEK293T cells. After the membrane break-in, slow development of outwardly rectifying ANO6 current was observed. The approximate time required to reach peak amplitude (t_{peak}) of the I_{ANO6} was about 220 s, with spontaneous inactivation after reaching the peak level (Fig. 1a and 1b, see Fig. 3 for a quantitative summary). To exclude the possibility that the delayed activation of I_{ANO6} was caused by poor access conductance with diffusional limitation of pipette Ca^{2+} ions, I also performed patch clamp with ANO1-overexpressing HEK293T cells using 1 μM and 10 μM $[Ca^{2+}]_i$. However, the delayed activation was not observed in ANO1 expressed HEK293T cells (Fig. 2). In contrast to the whole-cell configuration, inside-out patch of ANO6 showed instantaneous activation of I_{ANO6} by implying 10 μM $[Ca^{2+}]$ at cytoplasmic side (Fig. 1c and 1d).

Acceleration of I_{ANO6} activation and inactivation by actin depolymerization

To determine the role of the actin cytoskeleton on I_{ANO6} activation, ANO6 V1-expressed HEK293T cells were pretreated with 30 μM cytoD for 1 h, which depolymerized actin by binding to F-actin polymer[38]. As shown in Fig 3a, cytoD pretreatment on ANO6-expressed cells induced significantly faster activation compared to control cells (t_{peak}, 24.6 ± 4.7 s, n=10, Fig. 3a and 3d). The peak current density of I_{ANO6} was 163.2 ±22.1 pA/pF (n=9) and 94.3 ± 18.7 pA/pF (n=10) with and without cytoD pretreatment, respectively (Fig. 3f). However, owing to the wide range of the values, the significance of cytoD effects on the peak current density could not be determined (P value > 0.05). In contrast to cytoD effects, pretreatment with the microtubule inhibitor colchicine (10 μM for 1 h) did not change t_{peak} of I_{ANO6} (265 ± 121.7 s, n=4, Fig. 3d) as well as the peak current (59.7 ± 18.3 pA/pF, Fig. 3f). Notably, the inactivation of I_{ANO6} followed by its peak level was accelerated and more severe by cytoD pretreatment (Fig. 3a and 3e). The normalized decline ratio of I_{ANO6} at 60 s from the peak level (I/I_{peak} %) was 27 ± 4.7 % and 60.4 ± 7.5 % without and with cytoD pretreatment, respectively.

Actin filament stabilizers showed dramatic inhibitory effects on I_{ANO6}. Treatment with phalloidin (100 μM in pipette solution, stabilizing polymerized actin) or pretreatment with jasplakinolide (100 nM for 1 h, promoting polymerization), no significant I_{ANO6} was induced with 10 μM Ca^{2+} in the pipette solution during

1 5

relatively long prolonged time 10 min (Fig. 3b, 3c and 3f).

Next, the structural changes of the actin filaments of ANO6-expressed HEK293T cells treated with cytoD and Ca^{2+} ionophore (10 μM ionomycin for 15 min) were confirmed by using immunocytochemistry. The actin filaments were visualized by phalloidin-FITC staining using confocal microscopy. In contrast to the well-organized cortical actin structure in control cells, cytoD-treated cells showed severe derangement of the cortical actin cytoskeleton (Fig. 4a and 4b). Sustained Ca^{2+}-overloading by treatment with ionomycin also disorganized the cortical actin filament structures, although less severely than the cytoD (Fig. 4c). A previous study has reported that serotonin-specific reuptake inhibitors (SSRI) could significantly accelerate the activation of I_{ANO6}[24]. Interestingly, treatment with fluoxetine (30 μM for 15 min) also induced disruption of the cortical actin structure (Fig. 4d).

Deceleration of I_{ANO6} activation by intracellular ATP in actin filament-dependent manner

To investigate the effects of intracellular ATP on I_{ANO6}, the whole-cell patch recordings were performed with pipette solution containing 3 mM MgATP and 10 μM $[Ca^{2+}]$. The t_{peak} of I_{ANO6} with MgATP was significantly longer than the control without MgATP (820 ± 163.7 s vs. 222.4 ± 25.8 s, Fig. 5a and 5d). When I used

3 mM Na$_2$ATP instead of MgATP in the pipette solution without adding Mg^{2+}, the activation kinetics of I$_{ANO6}$ (t_{peak}), was similar to the control recordings (Fig. 5b and 5d). Interestingly, even in the presence of MgATP, cytoD pretreatment could still shorten the t_{peak} of I$_{ANO6}$ (45.7 ± 3.7 s, Fig. 5c and 5d). In some cases of whole-cell recordings, weakly outwardly rectifying anionic current was transiently activated in the initial period after membrane break-in (Fig. 4a and Fig. 6). Such conductance was supposedly an activation of volume-regulated anion current due to putative osmotic imbalance in the initial period of intracellular dialysis. Here, I did not count the initial transient increase of semi-linear current as I$_{ANO6}$. The inactivation of I$_{ANO6}$ was also affected by MgATP as almost non spontaneous decay existed in presence of MgATP (3.1 ± 1 % decline at 60 s after t_{peak}) (Fig. 5a and 5e). With Na$_2$ATP instead of MgATP, the inactivation was similar to that in ATP-free condition along with the effects on t_{peak} (Fig. 5b and 5e). However, even with MgATP, cytoD treatment induced prominent inactivation of I$_{ANO6}$ (81.6 ± 7.5 % decline within 60 s, Fig. 5c and 5e). Although the peak amplitudes of I$_{ANO6}$ tended to increase with MgATP and Na$_2$ATP, statistical significance could not be determined (Fig. 5f).
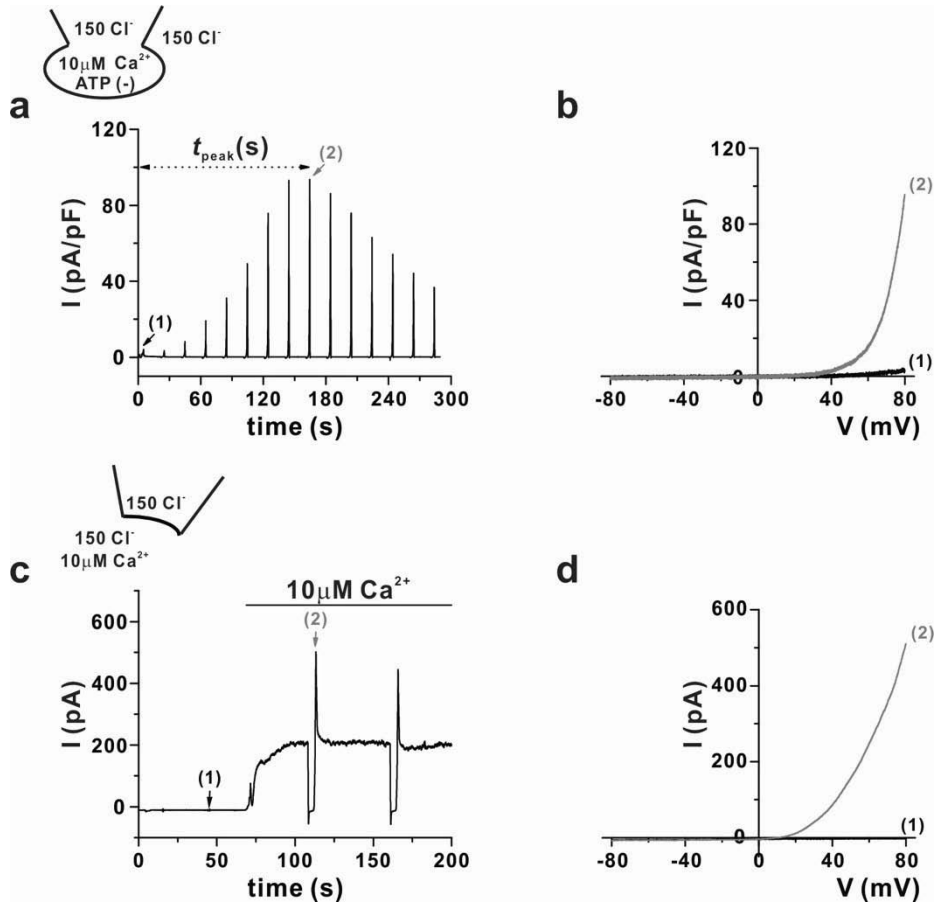
Figure 1. Comparison of I_{ANO6} activation between whole-cell and inside-out patch recordings

(a), Representative current traces of ANO6 (I_{ANO6}) in whole-cell patch clamp with 10 μM free calcium in ATP-free pipette solution from ANO6-transfected HEK293T cells. A ramp-like pulse from −80 mV to 80 mV (duration time 3 s) was applied every 20 s (holding voltage, −60 mV). (b), Current (I)−voltage (V) relationship curve obtained from initial point (1) and peak current amplitude (I_{peak}) (2) of the whole-cell patch. (c), Representative macroscopic currents of I_{ANO6} in an inside-out patch clamp. The membrane voltage was clamped at 60 mV with intermittent ramp pulses to confirm the outwardly rectifying I/V curve. (d), I−V relationship curve obtained from calcium-free condition (1) and I_{ANO6} with 10 μM Ca^{2+} (2) of the inside-out out patch.
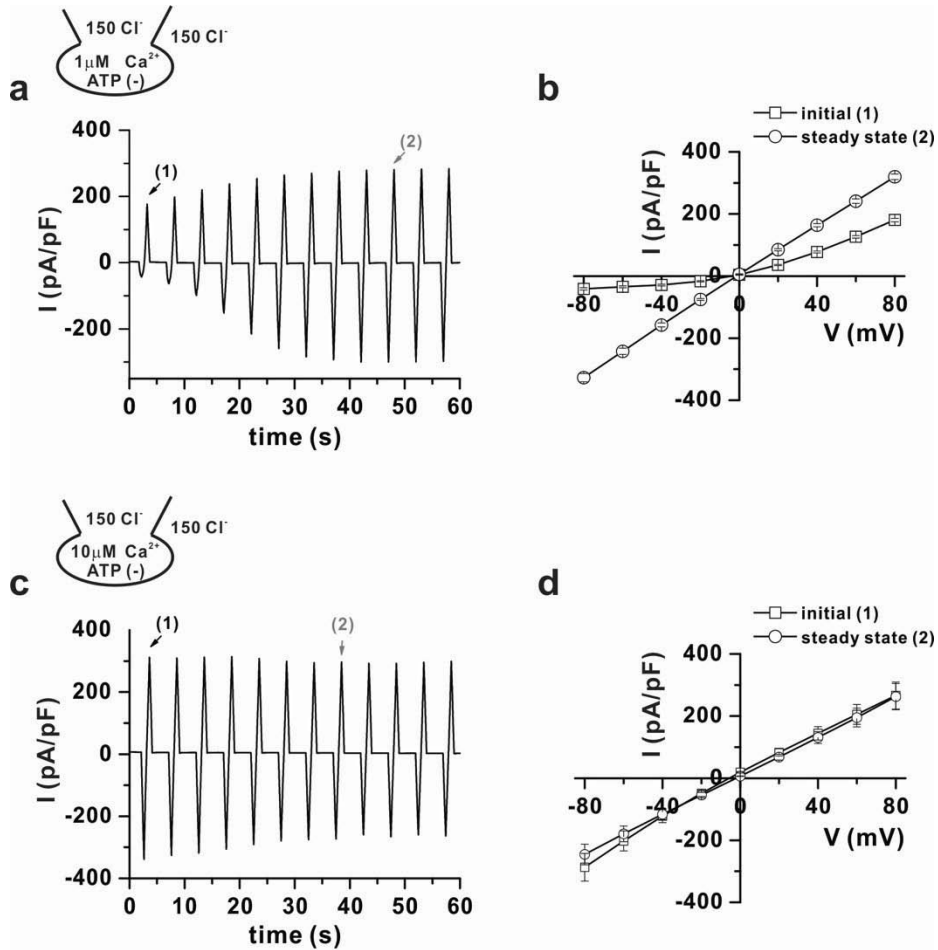
Figure 2. ANO1 whole-cell current with 1 μM and 10 μM $[Ca^{2+}]_i$

(a) and (c), Representative current traces of ANO1 generation in whole-cell patch clamp with 1 μM and 10 μM cytosolic free calcium, respectively. (b) and (d), Mean current (I)-voltage (V) relation curve obtained from initial point (1) and I_{steady} (2) of the whole-cell patch clamp with 1 μM and 10 μM free calcium, respectively (n=4).
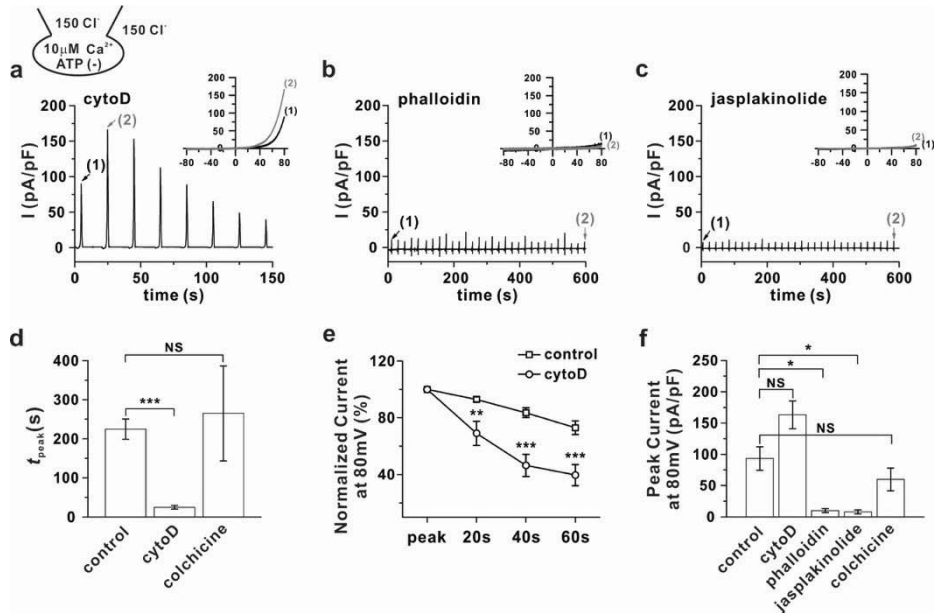
Figure 3. Actin cytoskeleton altered activation and inactivation of I_{ANO6}

(a–c), Representative current traces of I_{ANO6} generated from ANO6-expressed HEK293T cells treated with the indicated cytoskeleton disrupters or stabilizers. (a) Cells were treated with cytoD, (b) whole-cell currents recorded with 100 μM phalloidin in the pipette solution, and (c) cells were treated with jasplakinolide. Relative I–V relationship for initial current (1, black arrow) and I_{peak} (2, gray arrow) is presented in the upper right panel of each representative trace. (d), Summary bar graph of t_{peak} of I_{ANO6} estimated from whole-cell patch recording from cytoD and colchicine treated cells. (e), Remaining currents normalized to peak currents (%) at 20 s, 40 s, and 60 s after the peak currents (square-control; circle-cytoD). (f), I_{peak} elicited by + 80 mV holding potential in each group. Data represent the mean ± SEM. NS indicates not significant, * $P < 0.05$, ** $P < 0.01$, *** $P < 0.001$ vs. control.
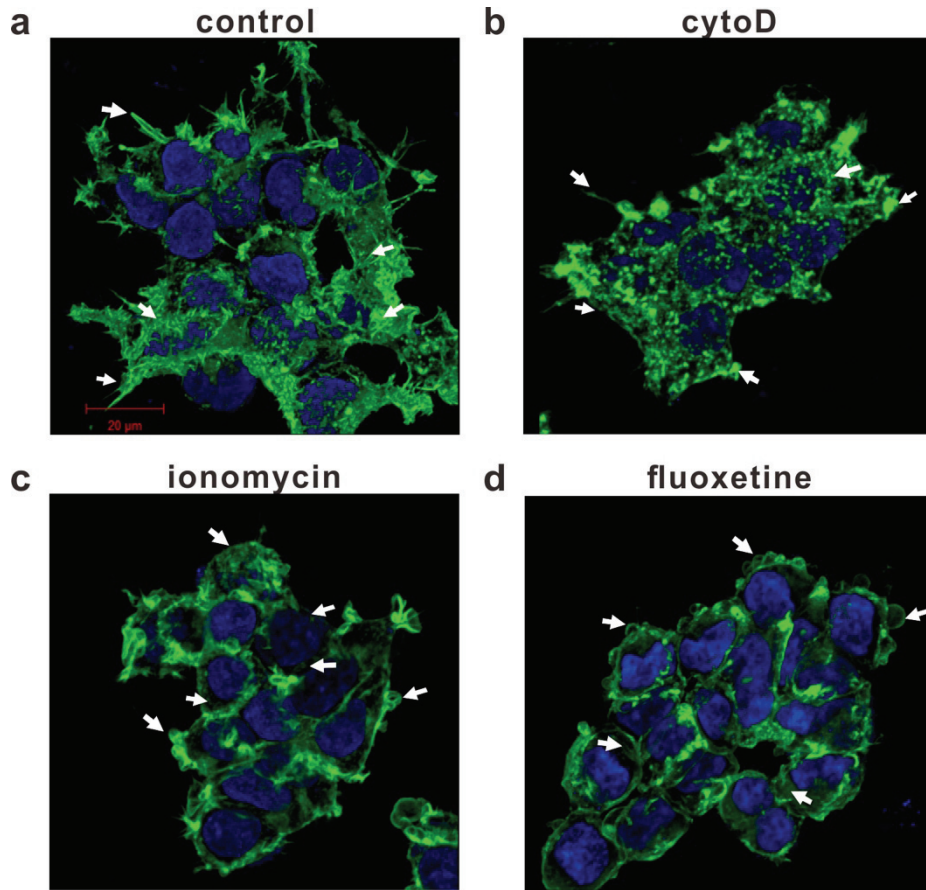
Figure 4. High cytosolic calcium and fluoxetine disrupt cortical actin cytoskeleton

Representative immunocytochemistry images of phalloidin-FITC (green) and DAPI (blue) in ANO6-expressing HEK293T cells treated with (a), 30 μM cytoD (b), 10 μM ionomycin (c), 30 μM fluoxetine (d). Original magnification, 63×. Scale bars, 20 μm.
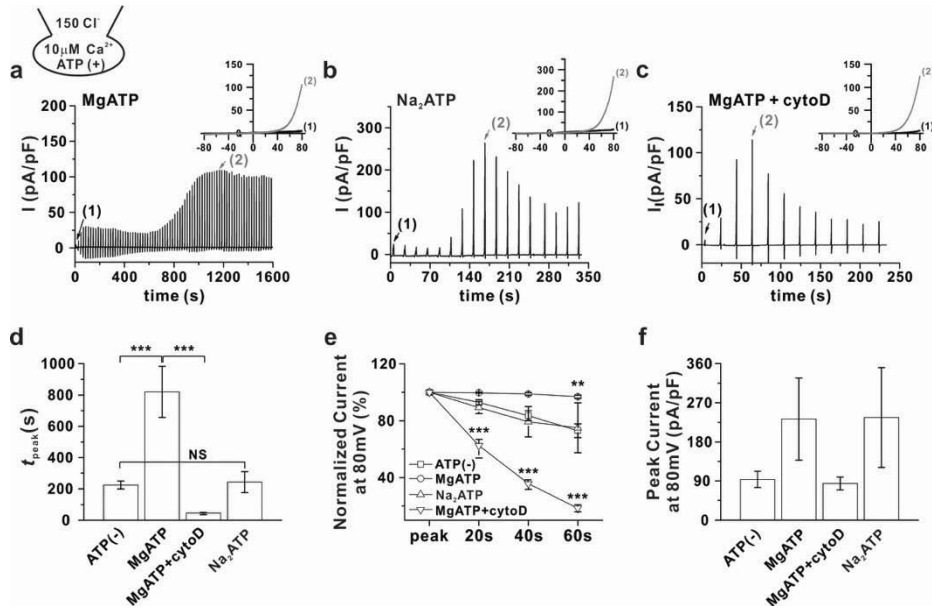
Figure 5. Cytosolic MgATP regulates ANO6 channel activity through the actin cytoskeleton

(a–c), Representative current traces of I_{ANO6} generated from ANO6-expressed HEK293T cells with 10 μM free Ca^{2+}, 3 mM MgATP-containing pipette solution (a), with 10 μM free Ca^{2+}, 3 mM Na_2ATP-containing pipette solution (b) and 30 μM cytoD-pretreated cells with 10 μM free Ca^{2+}, 3 mM MgATP-containing pipette solution (c). Relative I–V relationship for initial current (1, black arrow) and I_{peak} (2, gray arrow) is presented in the upper right panel. (d), Summary bar graph of t_{peak} of I_{ANO6} estimated from the whole-cell patch recordings of each group. (e), Remaining currents normalized to peak currents (%) at 20 s, 40 s and 60 s after the peak currents (square-control; circle-MgATP; triangle-Na_2ATP; inverted triangle-MgATP + cytoD). (f), Peak currents elicited by + 80 mV holding potential in each group. Data represent the mean ± SEM (n=4 for MgATP, n=7 for MgATP + cytoD, n=6 for Na_2ATP). NS indicates not significant, ∗ $P < 0.05$, ∗∗ $P < 0.01$, ∗∗∗ $P < 0.001$ vs. control.
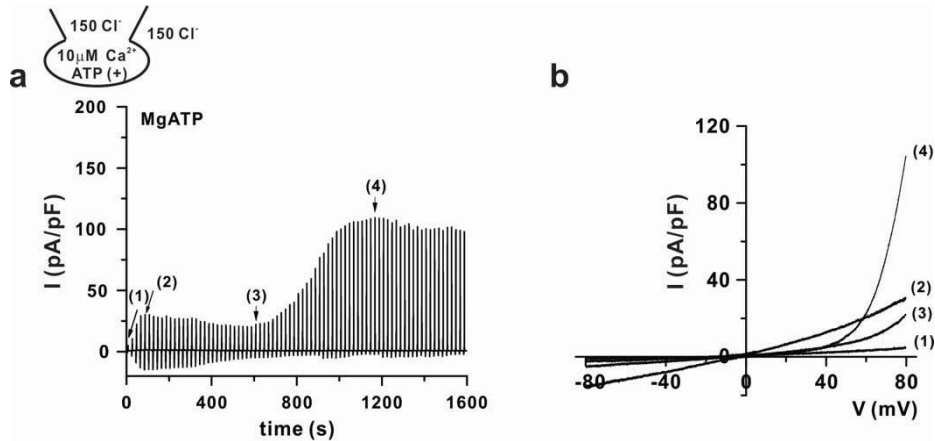
Figure 6. ANO6 channel activation accompanied by early appearance of VRAC-like current

(a), Representative current traces of I_{ANO6} generated from ANO6-expressing HEK293T cells in pipette solution containing 10 μM free Ca^{2+} and 3mM MgATP. (b), Relative I-V relationship between initial current (1) and VRAC-like current (2) and between $I_{ANO6-initial}$ current (3) and $I_{ANO6-peak}$ current (4).

Discussion

The pharmacological agents which affect the actin cytoskeleton had dramatic effects on the activation of I_{ANO6}. This result suggested that weakening or depolymerization of actin filaments might be required for ANO6 activation, even with high levels of $[Ca^{2+}]_i$. The instantaneous activation of ANO6 by Ca^{2+} in excised membrane patches is consistent with this interpretation. Because cytoD but not colchicine affected the I_{ANO6}, the regulatory effects appeared be confined to actin cytoskeleton disruption. Although there are numerous cases of ion channel regulation by actin filaments[39], the present study is the first to report on the inhibitory role of actin filaments on ANO6.

Inactivation of I_{ANO6} was also facilitated by cytoD, suggesting putative dual roles of actin filaments in the two different processes of ANO6 regulation, i.e., activation and inactivation. It is possible that after treatment with cytoD, the excessive Ca^{2+} loading to the cytosol might further aggravate the intracellular conditions for maintaining functional ANO6 in the plasma membrane. Although further investigation is definitely necessary, the spontaneous inactivation of ANO6 might reflect a negative feedback mechanism to prevent excessive activation in Ca^{2+}-overloaded conditions[33].

Ye et al., a recent paper showed that phosphatidylinositol-(4,5)-bisphosphate (PIP$_2$) prevents the desensitization of calcium response of ANO6, and MgATP showed the same effects as PIP2

for ANO6 activity[33]. The prevention of inactivation by MgATP but not by Na_2ATP in this study seems to be consistent with the findings reported by Ye et al. (Fig. 5a and 5b). However, it has to be noted that their study focused on I_{ANO6} recorded in inside-out patch while this study focused on current recordings in whole-cell patch, therefore, the role of actin filaments could be better revealed in my study. For the actin polymerization process, it is well known that ATP, especially MgATP, is indispensable[40,41]. In this respect, one might interpret that the delayed activation of I_{ANO6} by MgATP could be owing to a better preservation of actin filaments. Even in the presence of MgATP, cytoD treatment accelerated both activation and inactivation, indicating relatively dominant roles of actin filaments.

However, it has to be considered that PIP_2 is a regulator of actin polymerization and a platform provider for cytoskeleton/ membrane linkages[42]. In this respect, ANO6 might be regulated by the actin cytoskeleton and PIP_2 in a concerted manner, where the presence of MgATP contributes to both mechanisms. However, to elucidate the precise regulatory mechanism, further study, including on the interactions with Rho GTPases, which are important mediators between actin and PIP_2 in relation to actin cytoskeleton polymerization, is needed[43]. For example, Rho GTPases might be involved in the results observed in present

2 5

study. I suggest that both roles of actin cytoskeleton and PIP_2 should be considered to understand the regulation of ANO6.

  The scramblase action of ANO6 induces phosphatidylserine (PS) exposure in the process of platelet aggregation or apoptosis[44]. In addition, the scramblase activity is associated with the formation of plasma membrane blebs and microparticles[45,46]. For the membrane blebbing phenomenon, local weakening of the connection between the plasma membrane and the cortical actin cytoskeleton would precede and might be followed by PS exposure[46,47]. Therefore, I cautiously suggest that the facilitation of ANO6 by actin filament disruption might reflect the linked roles of ANO6 in membrane blebbing and PS exposure. However, because I only measured anion conductance changes, further investigation is requested to elucidate the precise mechanisms of scramblase activation in the context of actin cytoskeletal changes. Actin cytoskeleton staining revealed that the cortical actin cytoskeleton is destroyed by increased $[Ca^{2+}]_i$. Interestingly, I found that fluoxetine dispersed the cortical actin filaments, and this negative effect of fluoxetine treatment on the actin filament structure might explain the previous finding of accelerated activation of I_{ANO6} by fluoxetine and other SSRIs[24].Although further investigation is necessary, the effect of fluoxetine on the cytoskeletal structure might, at least in part, also be mediated by these signaling mechanisms. Present finding that the actin

cytoskeleton can regulate ANO6 activation and inactivation provides important novel clues to further elucidate ANO6 regulating mechanisms and the associated lipid scramblase activity in future.

Part 2. Temperature-dependent increase in the calcium sensitivity and acceleration of ANO6 activation

Introduction

First part of the study focused on the delayed activation property of ANO6, and revealed that the actin cytoskeleton and intracellular MgATP negatively regulated ANO6 channel kinetics. ANO6 has four alternative splicing variants, and most previous studies including first part of this study, have dealt with variant type 1 (V1). According to a recent study, three types variants (V1, V2, and V5) of ANO6 show CaCC activity with differential Ca^{2+} sensitivity and time delay for peak current generation: V2 showed a shorter delayed time than V1 and V5, whereas V2 andV5 showed a higher Ca^{2+} sensitivity than V1. However, even the relatively more sensitive variants of ANO6 (V2 and V5) still required several micromolar $[Ca^{2+}]_i$ and over than 100 s delayed time for significant activation to be detected[25]. So, because of this peculiar activation property of ANO6, the physiological role of ANO6 as an ion channel is still controversial.

  The experimental temperature generally affects the activities of ion channels by increasing the maximum current amplitudes and

kinetics of activation/inactivation[48,49]. In response to a temperature change, ANO1 showed increased activated current densities, with a Q_{10} (the 10°C temperature coefficient) value of approximately 19.4, and an increase in the $[Ca^{2+}]_i$ lowered the temperature threshold for ANO1 activation[5]. Based on this background, I hypothesized that the low Ca^{2+} sensitivity and the delayed activation of ANO6 might be due to the experimental temperature (i.e., room temperature) applied in previous studies. Therefore, this part of study investigated the effects of physiological temperature (37°C) on the activity of ANO6 variants in terms of their Ca^{2+} sensitivity and delayed activation. Due to the intracellular MgATP affect the activation kinetics of ANO6, in this study, the intracellular ATP was sustained with 1mM MgATP contained in pipette solution, which concentration affiliated to the physiological range. I found that although each variant differed, all could be activated at temperatures between 37–42°C under sub-micromolar Ca^{2+} concentrations with short delays. In contrast, the $[Ca^{2+}]_i$-dependent scramblase activity of ANO6 was not altered. This work is expected to clarify the role of ANO6 as a chloride channel in physiological conditions beyond its known function as a scramblase.

Results

Membrane expression and ion channel activity of ANO6 variants

Firstly, the membrane localization of ANO6 variants was confirmed by using surface biotinylation assay in ANO6 variants-expressed HEK293T cells. The results indicated insignificant membrane expression of ANO6 V3 (Fig. 7a). The membrane expression of V1 was higher than that of V2, with an intermediate level of V5 (Fig. 7a and 7b). The molecular sizes of ANO6 variants in the cytosolic fraction appeared to reflect differential glycosylated states, with the Golgi-mediated complex in its glycosylated form being detected in the surface biotinylation assay (Fig. 7a). To confirm ANO6 variant functional activity, a whole-cell patch clamp was conducted for mock (GFP), V1, V2, V3, and V5 of ANO6-transfected HEK293T cells using symmetrical NMDG-Cl solutions with 100 μM $[Ca^{2+}]_i$ which is known as the maximal Ca^{2+} concentration for ANO6 variant activation[28]. The step pulse protocol used for ANO6 channel recordings, is started from holding potential of -60 mV and depolarized for 0.5 s from -100 mV to +100 mV with 20 mV increments and a ramp-like depolarization from -100 mV to +100 mV was applied at every 20 s after the membrane break-into attain the whole-cell configuration. As shown in Figure 8a and 8b,

V1, V2, and V5 transfected into HEK293T cells produced outwardly rectifying chloride current (I_{ANO6}) at 100 μM $[Ca^{2+}]_i$, whereas V3 elicited insignificant membrane currents with the same level as mock. Even in maximal $[Ca^{2+}]_i$, ANO6 variants showed characteristic delayed activation, with the different time delays to reach the peak amplitude (t_{peak}) being 290.9 ± 36.9, 49.1 ± 6.2, and 72 ± 9 s for V1, V2, and V5, respectively (Fig. 8c).

Temperature-dependent increase of the Ca^{2+} sensitivity of ANO6

A whole-cell voltage clamp was conducted for V1, V2, and V5 of ANO6-transfected HEK293T cells with 1 μM $[Ca^{2+}]_i$. None of the variants was activated by 1 μM $[Ca^{2+}]_i$ at 27°C, given that no currents were generated, even over long-term (15 min) recordings, as observed by Scudieri et al. (2015)[25] (Fig. 9a and 9c). In contrast, at 37°C, V1, V2, and V5 generated I_{ANO6} with 1 μM $[Ca^{2+}]_i$ (Fig. 9b and 9c). t_{peak} of I_{ANO6} was significantly longer in V1 than in V2 and V5 (Fig. 9d, Table 1). In addition, the temperature effect on I_{ANO6} was reversible. After confirming the full activation of I_{ANO6}, changing the bath perfusate to one equilibrated with 27°C readily decreased the current amplitude, whereas upon subsequent change back to 37°C, the currents increased without delayed activation, activating almost in the same time as the rate

of bath temperature exchange in 60–70 s (Fig. 10a). It was notable that the recovery of I_{ANO6} was almost completed (Fig. 10b). One peculiarity is that there is a difference in size between the variants, but once activated at 37°C, I_{ANO6} is still active at 27°C. In particular, V5 showed 30 % activity at + 100 mV compared to I_{ANO6} at 37°C.

 Although the ANO6 variants could be activated even with 1 μM $[Ca^{2+}]_i$, the initial appearance of I_{ANO6} and steady-state activation took a considerable amount of time; such abnormally long sustained high calcium conditions would occur only under pathological conditions. Thus, I next asked whether raising the temperature to physiological values would induce I_{ANO6} at the submicromolar range of $[Ca^{2+}]_i$ in HEK293T cells expressing V1, V2, or V5. In particular, with 300 nM of $[Ca^{2+}]_i$ at 37°C, V2 and V5 showed significant I_{ANO6} activation. However, V1-expressing cells did not show any current activation up to 900 s after the membrane break-in (Fig. 11a and 11c, Table 1). To identify whether an increased temperature could activate V1, the temperature was raised up to 42°C. As shown in Figure 11b, increasing the temperature to 42°C could activate all ANO6 variants. However, t_{peak} was not significantly decreased (Fig. 11d). Interestingly, when the $[Ca^{2+}]_i$ was further lowered to 100 nM, close to the resting $[Ca^{2+}]_i$, ANO6 variants V2 and V5 generated very small and partially activated outward currents at 37°C (11~15 pA/pF at =100 mV), whereas V1 did not (Fig. 12a and 12c),

and at 42℃, V1 showed slightly activated outward currents when V2 and V5 still generated small but significant outward rectifying currents, as the currents elicited at + 100 mV I_{ANO6} were about 21.7 ± 3.9, 73.9 ± 10.8, and 53.4 ± 25.7 pA/pF for V1, V2, and V5, respectively (Fig. 12b and 12c). However, all ANO6 variants did not generate any current in a calcium-free pipette solution even at 42℃ (Fig. 13).

Temperature-dependent acceleration of ANO6 activation

To compare the change of t_{peak} according to the temperature change under the condition of I_{ANO6} activation at 27℃, $[Ca^{2+}]_i$ was fixed at 3 μM and whole-cell patch clamp was conducted. In all the three variants, I_{ANO6} reached the peak amplitude faster at 37℃ than at 27℃ (Fig. 14a, 14b, and 14d, Table 1). Among the variants, the activation speed of V1 was generally slower than that of V2 and V5 at both temperatures (Fig. 14d), whereas t_{peak} was reduced to approximately 40–50 % by increasing the temperature from 27℃ to 37℃ in all variants. However, in case of the peak current generation, V1 showed almost no change in peak current amplitude due to temperature change, and only V2 and V5 showed statistically significant increase in peak current amplitudes, about 1.7- and 1.8-fold increase, respectively (Fig. 14e). As reported by Kim et al., the human pancreatic carcinoma PANC-1 cells

endogenously express ANO6, produced ANO6-like currents with 10 μM $[Ca^{2+}]_i$, but not by 3 μM $[Ca^{2+}]_i$ at RT condition[24]. So, here, to identify whether the temperature effects also existed endogenously expressed ANO6, whole-cell patch recordings were performed in PANC-1 cells with 3 μM free calcium at 27°C and 37°C. Showed by Fig. 15, 37°C can induce I_{ANO6} like currents in PANC-1 cells.

Attenuated temperature-dependence of Ca^{2+}-sensitivity in the inside-out recording of ANO6

I also compared the effects of a serial increase of $[Ca^{2+}]_i$ (0.3, 1, and 3 μM) on I_{ANO6} under inside-out patch clamp conditions with symmetrical NMDG-Cl solution. After membrane excision, I_{ANO6} could be immediately activated by raising the $[Ca^{2+}]_i$ (Fig. 16). As shown in Figure 16a and 16b, although the bath solution temperature was increased to 37°C, all variants of ANO6 (V1, V2, and V5) were not activated by submicromolar range Ca^{2+} concentration (300 nM), which differed from the results of whole-cell patch recordings. However, at 1 μM free Ca^{2+} condition, V2 and V5 were significantly activated upon temperature increase to 37°C, whereas V1 activation did not reach significance. V2 and V5 showed approximately 25-fold increase versus those activated at 27°C, even though the current values were numerically small (V2 and V5 generated current values of 1.3 ± 0.8 and 2.6 ±1.2 pA at

27°C and 12.4 $\pm$ 4.9 and 32.2 $\pm$ 10.4 pA at 37°C, respectively).

In addition, the amplitude of I_{ANO6} of inside-out patch with 3 μM of $[Ca^{2+}]_i$ was significantly increased by raising the temperature by approximately 7-, 3-, and 4-fold for V1, V2, and V5, respectively (Fig. 16b), whereas I_{ANO6} in whole-cell patch recordings was less sensitive to the temperature increase, as V1 showed almost no change in peak current and V2 and V5 showed about 1.7- and 1.8-fold increase in peak current, respectively (Fig. 14e).

No significant role of PLA2 in the ANO6 activation

Recently, Schreiber et al. reported that ANO6 can be partially activated at 37°C even in intracellular Ca^{2+} free conditions, which might be due to the spontaneous activity of PLA2[50]. However, activation of PLA2 could not activate I_{ANO6} at a high intracellular Cl^- concentration, which inhibits I_{ANO6}[51]. Therefore, additional experiments were performed to determine whether PLA2 affects the temperature sensitivity of ANO6 variants. The experiment was conducted under two conditions: 150 and 30 mM intracellular Cl^- conditions. As shown in Fig 17a-d, in the 150 mM Cl^- condition, treatment with purified PLA2 (0.5 unit/ml), contained in a pipette solution, or 50 μM NEM (PLA2 activator) could not activate ANO6 variants at 27°C with 1 μM $[Ca^{2+}]_i$. Conversely, at 37°C, treating I_{ANO6} with the PLA2 inhibitor (ACA 20 μM and MAFP 5 μM) did not affect t_{peak} (Fig. 18a-c). Furthermore, in 30 mM Cl^- cytosolic

condition at 37°C with 1 μM $[Ca^{2+}]_i$, t_{peak} of I_{ANO6} variants were not affected by treatment with the PLA2 inhibitor (ACA 20 μM) (Fig. 19a–d). Moreover, ANO6 variants could not be activated, even at low cytosolic Cl⁻ at 37°C in resting intracellular Ca^{2+} (100 nM) (Fig. 20a–c).

Lower Ca^{2+}-sensitivity of the lipid scramblase function of ANO6 at physiological temperature

The notable increase in the Ca^{2+} sensitivity of I_{ANO6} at 37°C raised a question as to whether the scramblase activities of the ANO6 variants are similarly enhanced under the physiological temperature. Thus, a scramblase assay was conducted in the V1–, V2–, and V5–overexpressed HEK293T cells treated with ionomycin, a Ca^{2+}-ionophore. To determine the level of ionomycin treatment corresponding to the approximate $[Ca^{2+}]_i$ of 300 nM and 1 μM in intact cells, I measured the average $[Ca^{2+}]_i$ of the ANO6–overexpressed HEK293T cells using cuvette-type Fura-2 fluorometry. Various concentrations of ionomycin (0.01, 0.03, 0.1, 0.3, 0.6, and 1 μM) were applied to the cells, and the dose–dependent increase in $[Ca^{2+}]_i$ was fitted to a logistic function. Then I estimated the required ionomycin concentration to induce 300 nM and 1 μM $[Ca^{2+}]_i$ (Table 2). To avoid the binding of Annexin V to intracellular phosphatidylserine (PS) resulting from membrane damage, I compiled the statistics using only Annexin

3 6

V-positive/PI-negative cells (Fig. 21a). As shown in Fig. 21b, the scramblase activity of ANO6 was significantly increased within 15 min with 1 μM $[Ca^{2+}]_i$ at 37°C. However, no scramblase activity was detected under 300 nM $[Ca^{2+}]_i$ at 37°C for up to 30 min

Table 1. t_{peak}(s) of ANO6 variants with different Ca^{2+} concentrations at 27°C, 37°C, and 42°C (means ± SEM).

$[Ca^{2+}]_i$		V1	V2	V5
3 µM	27°C	906 ± 90	162 ± 30.9	114 ± 20
	37°C	485.7 ± 69.2	66 ± 7.9	45 ± 5
1 µM	27°C	N.R	N.R	N.R
	37°C	513.8 ± 72.9	75.7 ± 8.7	72.9 ± 8.2
300 nM	27°C	N.R	N.R	N.R
	37°C	N.R	174.3 ± 23.4	148.9 ± 27.3
	42°C	300 ± 180.9	112.5 ± 15.5	88.5 ± 17.9

N.R; No response

Table 2. Ionomycin concentrations (nM) for maintaining the $[Ca^{2+}]_i$ at 300 nM and 1 μM for each ANO6 variant (V1, V2, and V5) at 37°C.

$[Ca^{2+}]i$	300 nM	1 μM
V1	44.6	577
V2	35.8	538.5
V5	58.8	588.4

The concentrations were calculated from the non-linear curve fitting.

Figure 7. Membrane expression of hANO6 transcript variant V1, V2, V3, and V5

(a), A schematic comparison of the N-(upper panel) and C-terminus (lower panel) amino acids sequence of human ANO6 splicing variants (V1, V2, V3 and V5) based on the database from NCBI. The single underline means the difference sequence versus V1 (b), Surface biotinylation assay in HEK293T cells transfected with pcDNA3.1 expressing hANO6 V1, V2, V3, and V5. (c), Summary of membrane expression of each variant normalised to V1 (n=4). $* P < 0.05$, $*** P < 0.001$, compared to V1.
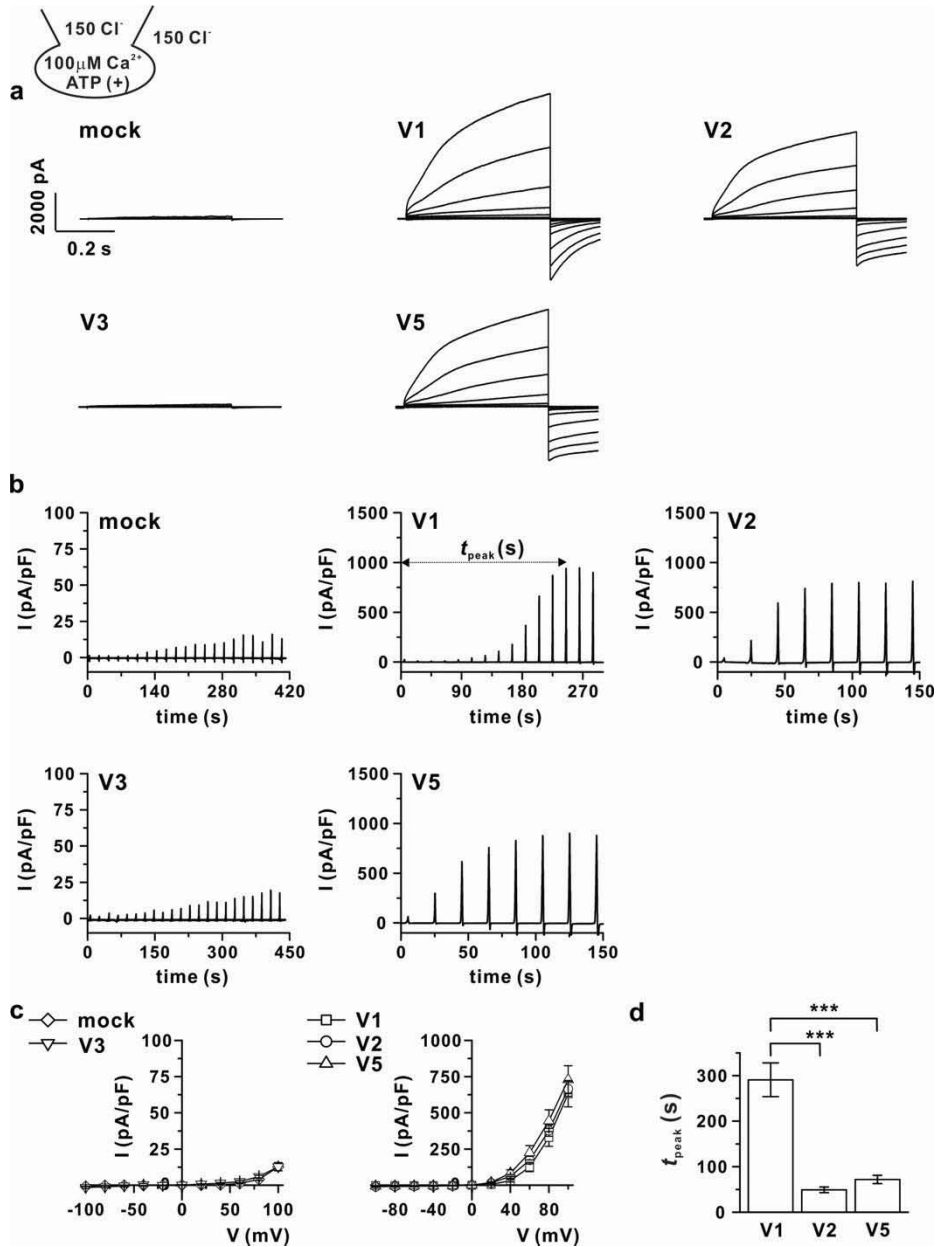
Figure 8. Membrane currents produced by hANO6 transcript variant V1, V2, V3, and V5

(a), Representative step pulse recordings of ANO6 currents (I_{ANO6}) with whole-cell patch clamping with 100 μM free calcium in pipette solution at 27°C for the mock (upper left panel), ANO6 variants V1 (upper middle panel), V2 (upper right panel), V3

4 1

(lower left panel), and V5 (lower right panel) expressed in HEK293T cells. (b), Representative ramp-like trace recordings of I_{ANO6} with 100 μM free calcium in pipette solution for the mock (upper left panel), ANO6 variants V1 (upper middle panel), V2 (upper right panel), V3 (lower left panel), and V5 (lower right panel) expressed in HEK293T cells. Under the whole-cell patch clamp, a ramp-like pulse from −100 mV to 100 mV (duration time 3 s) was applied every 20 s (holding voltage, −60 mV). (c), The peak corresponding current (I)–voltage (V) relationship curve obtained from mock-diamond and V3-down-triangle (left-panel), V1-square, V2-circle, V5-up-triangle (right-panel). (d), Summary bar graph of delay time (t_{peak}) of I_{ANO6} generation (the time from the start of whole-cell patch recordings to maximal current activation) detected with 100 μM $[Ca^{2+}]_i$. Data are presented as the means ± SEM (n=10 for V1, V2, and V5; n=4 for V3 and n=5 for mock). *** $P < 0.001$ compared to the control.
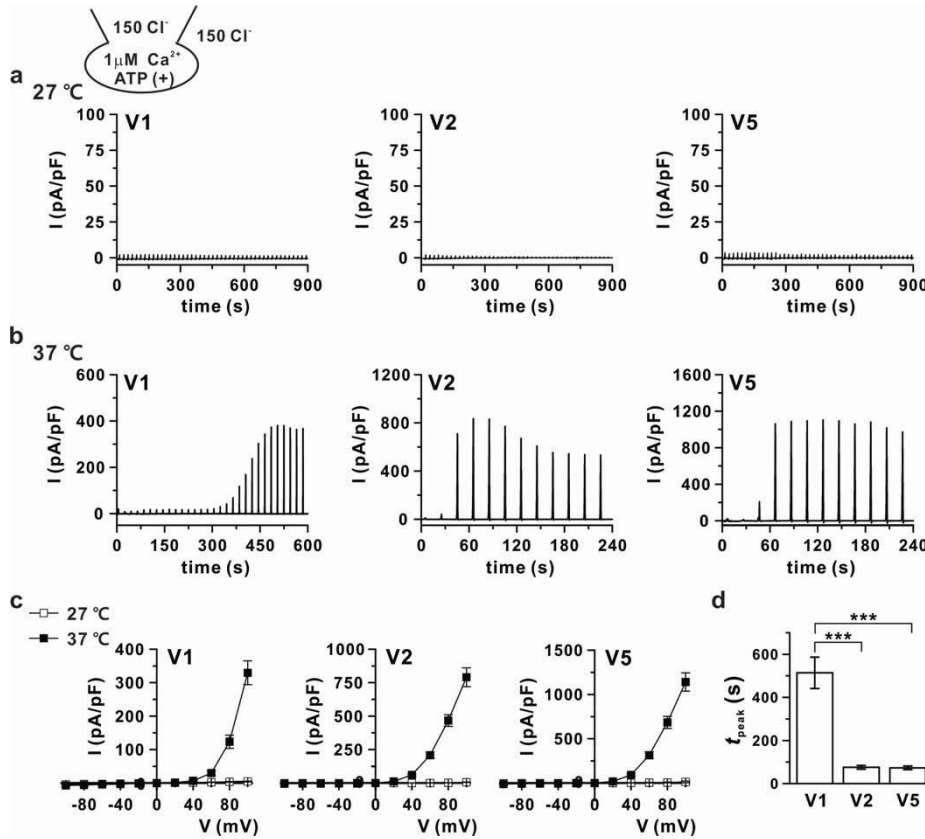
Figure 9. Increased calcium sensitivity of ANO6 variants at 37°C
(a) and (b), Representative traces of ANO6 currents (I_{ANO6}) with whole-cell patch clamping with 1 μM free calcium in pipette solution at 27°C (a) and 37°C (b) for the ANO6 variants V1 (left panel), V2 (middle panel), and V5 (right panel) expressed in HEK293T cells. The voltage protocol is already described in Fig. 8a. (c), I-V relation curve obtained from the peak current of each variant (V1-left panel, V2-middle panel, and V5-right panel) at 27°C (open-square) and 37°C (solid-square). (d), Summary bar graph of the t_{peak} of I_{ANO6} detected at 37°C. Data are are presented as the means ± SEM (n=13 for V1 and V2, n=15 for V5). *** $P <$ 0.001 compared to the control.
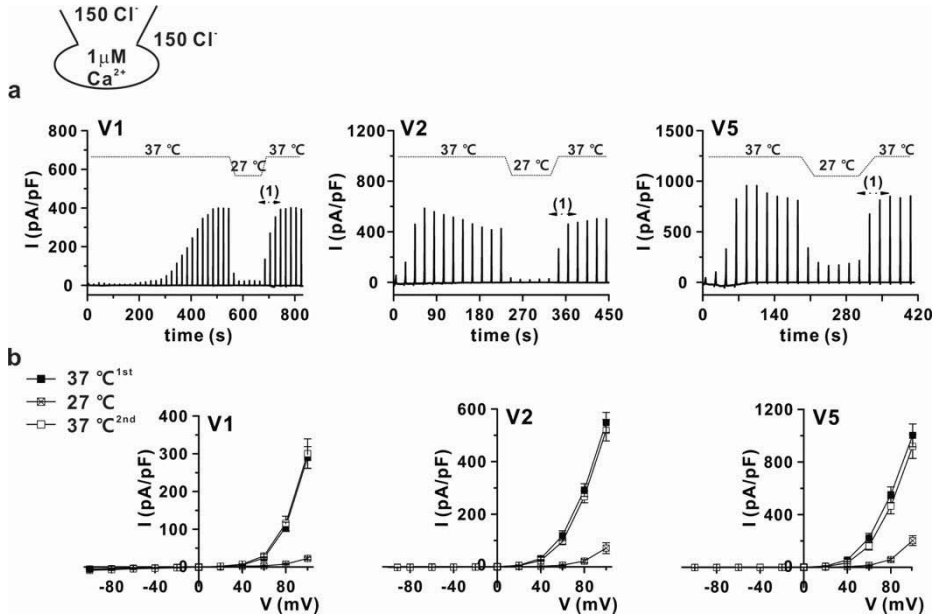
Figure 10. Reversible effect of temperature changes on I_{ANO6}
(a), Representative current traces of I_{ANO6} of each variant (ANO6 V1-left panel, V2-middle panel, and V5-right panel) expressed in HEK293T cells from 37°C to 27°C and returned to 37°C. (b), The peak current (I)-voltage (V) relationship curve of ANO6 variants V1 (left panel), V2 (middle panel), and V5 (right panel) detected at first 37°C (solid-square), 27°C (x, centre-square), and second 37°C (open-square). The same whole-cell patch protocol was used as described in Fig. 8 (n=8 for V1, n=6 for V2, and n=7 for V5).

44
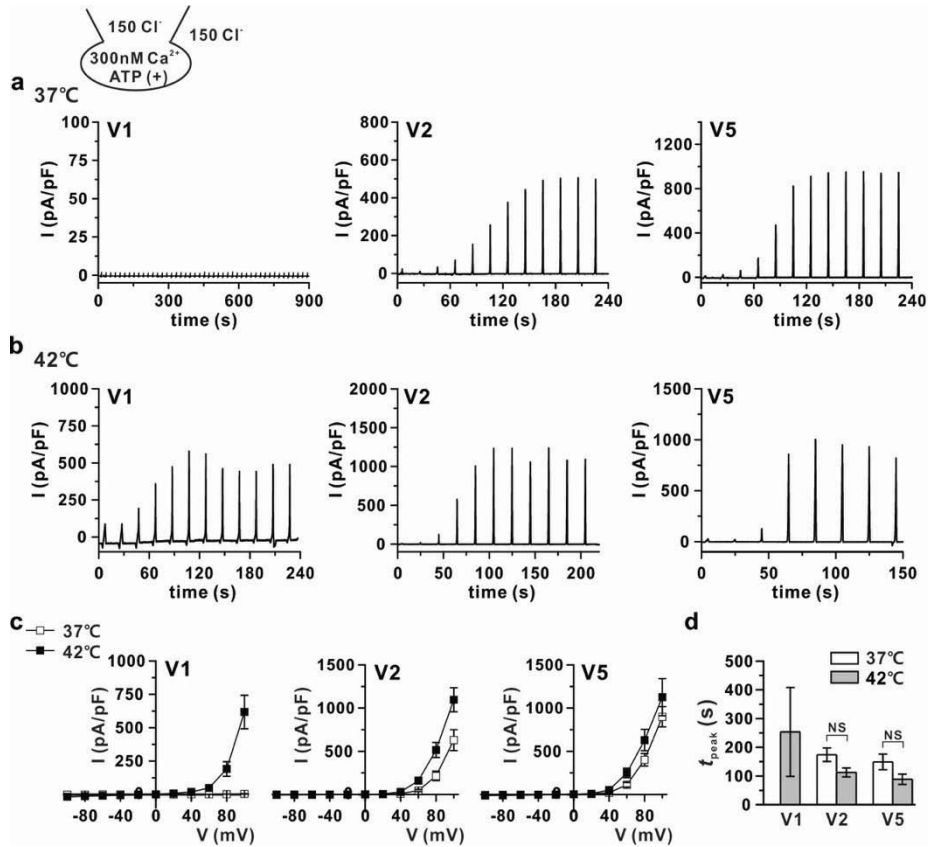
Figure 11. Temperature-dependent activation of ANO6 variants by submicromolar $[Ca^{2+}]_i$

(a) and (b), Representative trace of the I_{ANO6} of V1 (left), V2 (middle), and V5 (right) with 300 nM free calcium in pipette solution at 37°C (a) and 42°C (b) expressed in HEK293T cells. The pulse protocol is the same as that described in Fig. 8. (c), I–V relationship curves for the peak amplitude of each variant (V1-left, V2-middle, and V5-right) detected at 37 °C (open-square) and 42°C (solid-square) with 300 nM $[Ca^{2+}]_i$. (d), Summary bar graph of t_{peak} values of V1 detected at 37°C; V2 and V5 detected at 37°C and 42°C. Data are presented as the means ± SEM (n=4 for V1, n=7 for V2, and V5 at 37°C; n=5 for V1, n=8 for V2, and n=7 for V5 at 42°C).
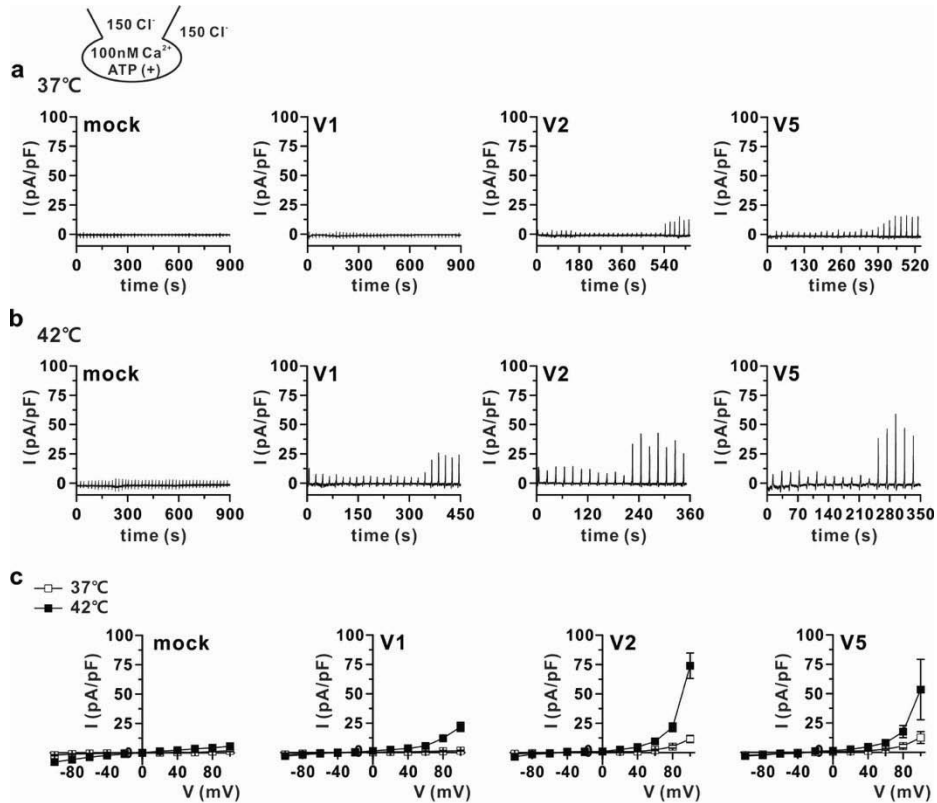
Figure 12. Partial activation of ANO6 variants 1, 2, and 5 by resting $[Ca^{2+}]_i$ at 42°C

(a) and (b), Representative trace of the I_{ANO6} of mock, V1, V2, and V5 at 37°C (a) and 42°C (b) with 100 nM $[Ca^{2+}]_i$ expressed in HEK293T cells. The pulse protocol is the same as that described in Fig. 8. (c), The peak I–V relationship curves obtained from mock and each variant detected at 37°C (open–square) and 42°C (solid–square) (n=5 for all variants at 37°C; n=4 for V1, n=7 for V2 and V5 at 42°C).

Figure 13. I_{ANO6} of variants 1, 2 and 5 detected under calcium-free condition at 42°C

(a), Representative trace of the I_{ANO6} of V1 (left-panel), V2 (middle-panel), and V5 (right-panel), in the presence of 0 $[Ca^{2+}]_i$, expressed in HEK293T cells. The pulse protocol is the same as that described in Fig. 8. (b,) I-V relationship curves obtained from V1 (square), V2 (circle), and V5 (up-triangle) (n=3 for all variants).
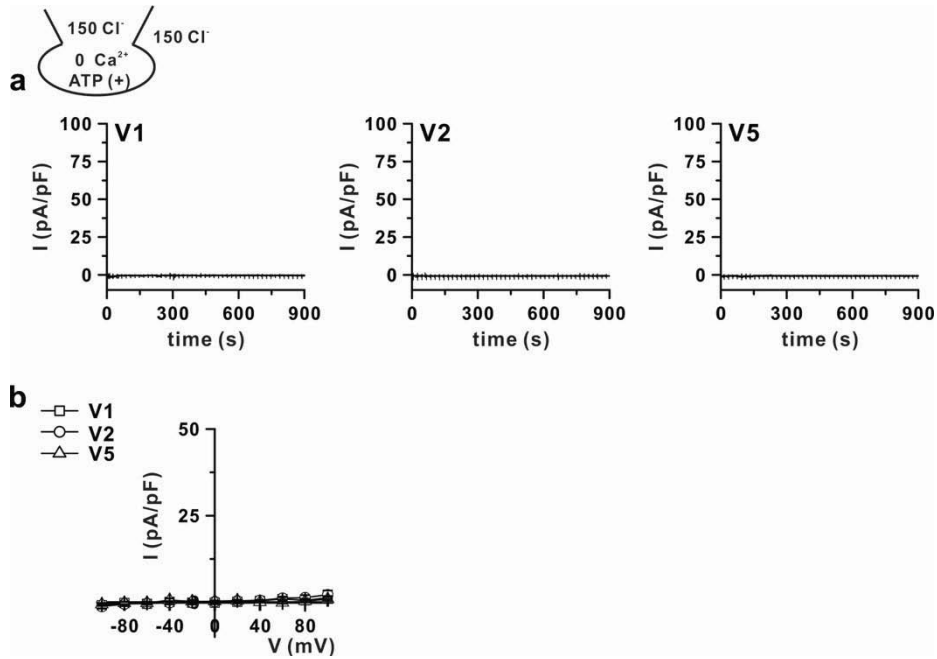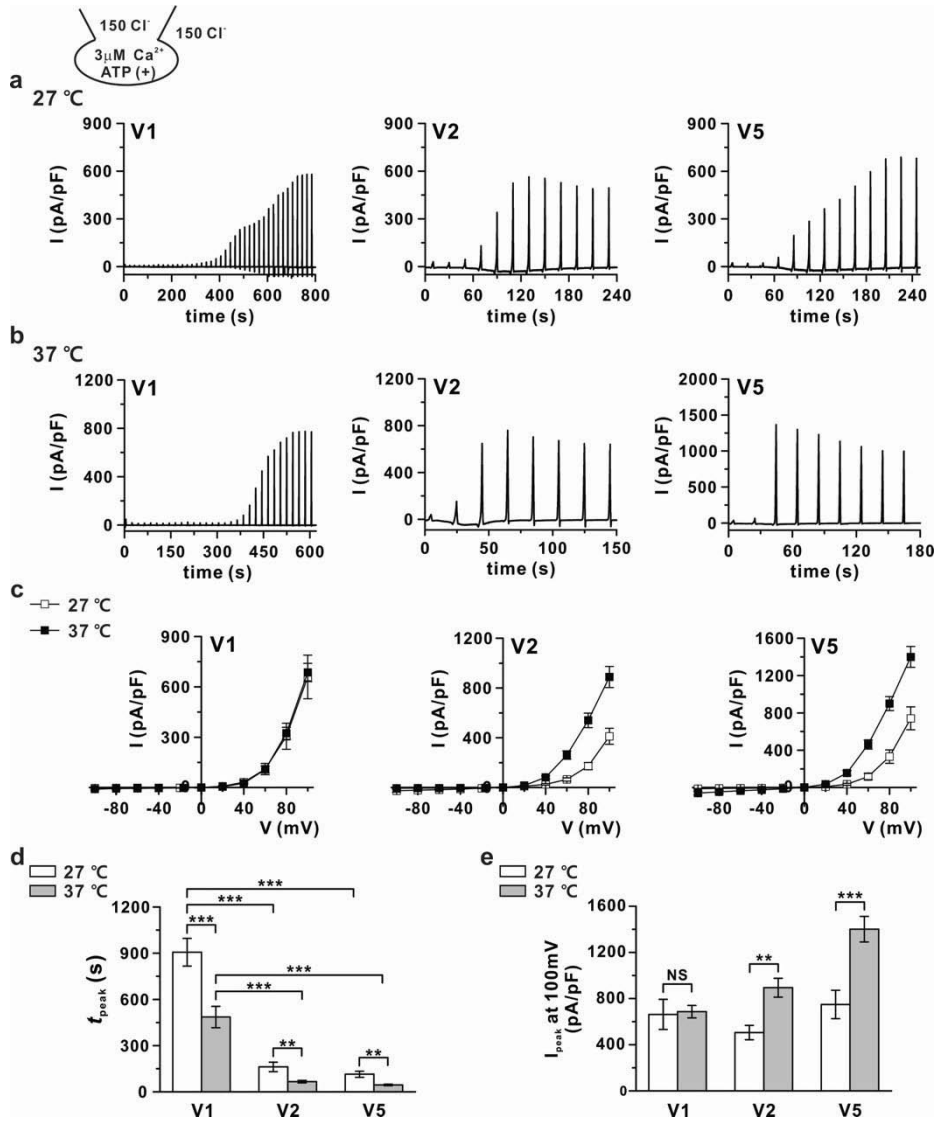
Figure 14. Accelerated activation of I_{ANO6} at 37°C

(a) and (b), Representative currents trace of I_{ANO6} generated from three variants (V1, left panel; V2, middle panel; and V5, right panel) with 3 μM free calcium in pipette solution at 27°C (a) and 37°C (b), respectively, in ANO6 variant-overexpressing HEK293T cells. The whole-cell patch recordings pulse protocol was the same as that described in Fig. 2. (c), Current (I) – voltage (V) relation curve obtained from the peak current of each variant detected at 27°C (open-square) and 37°C (solid-square). (d), Summary bar graph

of t_{peak} of I_{ANO6} of each variant estimated from the trace chart. (e), Peak currents elicited by 3 μM $[Ca^{2+}]_i$ at +100 mV holding potential from each variant at 27°C (white bar) and 37°C (grey bar), respectively. Data represent the means ± SEM (n=10 for 27°C and n=15 for 37°C, for all variants). NS indicates not significant, ** $P < 0.01$, *** $P < 0.001$ compared to the control.
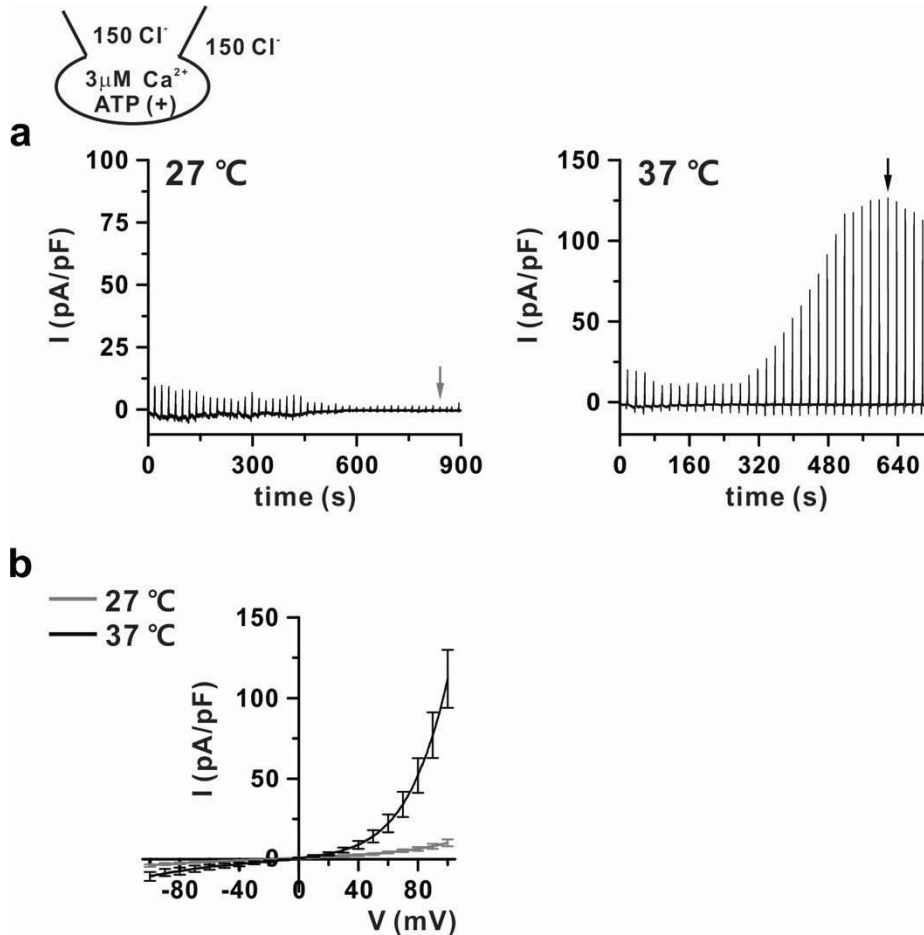
Figure 15. I_{ANO6} like currents detected in PANC-1 cells at 37°C
(a), Representative currents trace of I_{ANO6} generated from PANC-1 cells with 3 μM free calcium in pipette solution at 27°C-left panel and 37°C-right panel, respectively. The whole-cell patch recordings pulse protocol was the same as that described in Fig. 2. (b), The mean current (I)-voltage (V) relation curve obtained from the peak current of each variant detected at 27°C (gray) and 37°C (black) (n=11 for 27°C and n=13 for 37°C).
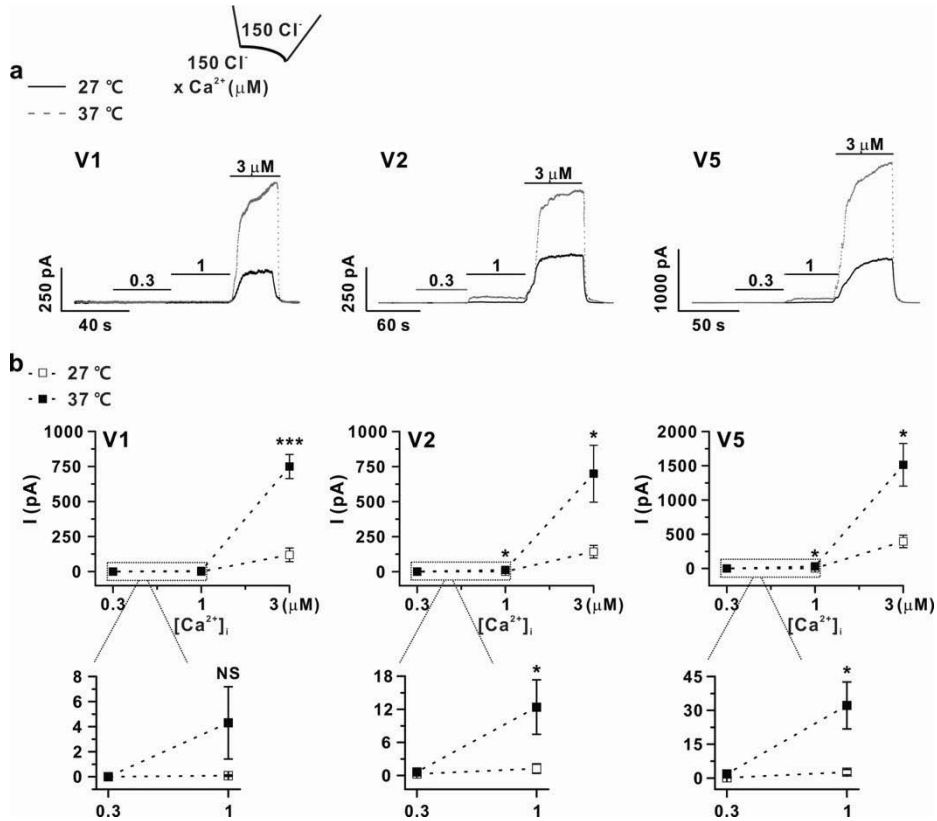
Figure 16. Calcium sensitivity and activation kinetics of ANO6 in excised patches

(**a**), Representative macroscopic currents of the I_{ANO6} of ANO6 variants V1 (left panel), V2 (middle panel), and V5 (right panel) in an inside-out patch clamp from ANO6 variant-transfected HEK293T cells. The patches were exposed for 40–60 s to Ca^{2+} concentrations of 300 nM, 1 μM, and 3 μM at a holding potential of +60 mV. (**b**), Statistics of the peak I_{ANO6} with different calcium concentrations at 27°C (open-square) and 37°C (solid-square); graphs displayed at the bottom represent the expansion of the boxed parts of the upper graphs. Data are presented as the means ± SEM (n=5 for V1, left; n=6 for V2, middle; and n=7 for V5, right). NS indicates not significant ∗ $P < 0.05$, ∗∗∗ $P < 0.001$ comparing current values at 37°C and 27°C.

5 1
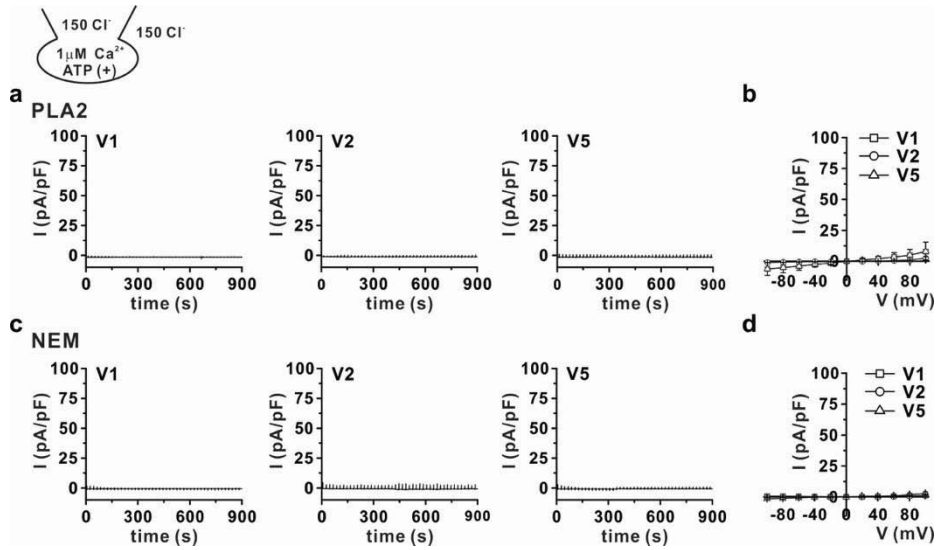
Figure 17. PLA2 effects on I_{ANO6} of variants 1, 2, and 5 under symmetrical Cl⁻ condition

(a) and (c), Representative currents trace of I_{ANO6} generated from the three variants (V1, left panel; V2, middle panel; and V5, right panel) at 27°C with 1 μM free calcium (a) 0.5 unit/ml PLA2 in pipette solution and (c) NEM (50 μM) treated, in ANO6 overexpressed HEK293T cells. (b) and (d), Current (I)−voltage (V) relation curve obtained from each variant detected at PLA2 in pipette (b) and NEM−treated conditions (d), respectively (V1−square, V2−circle, and V5−up−triangle). Data represent the means ± SEM (n=4 for V1, V2, and V5 for all conditions).
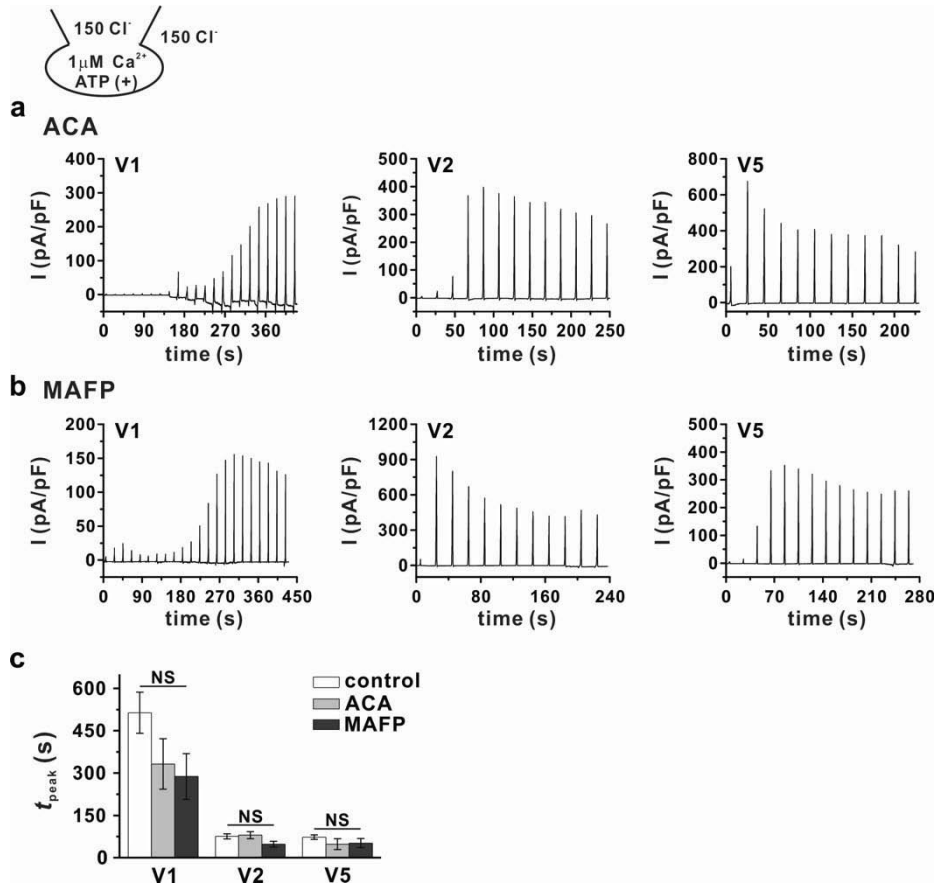
Figure 18. Effects of PLA2 inhibitors on I$_{ANO6}$ of variants 1, 2, and 5 under symmetrical Cl⁻ condition

(a) and (b), Representative currents trace of I$_{ANO6}$ generated from the three variants (V1, left panel; V2, middle panel; and V5, right panel) at 37°C with 1 μM free calcium ACA (20 μM)-treated (a) and MAFP (5 μM)-treated (b), respectively in ANO6 transfected HEK293T cells. (c), Summary bar graph of t_{peak} of I$_{ANO6}$ of each variant estimated from the trace chart of the control (Fig. 9b), ACA and MAFP treated conditions. Data represent the means ± SEM (n=5 for V1, V2, and V5 at all conditions). NS indicates not significant, compared to the control.
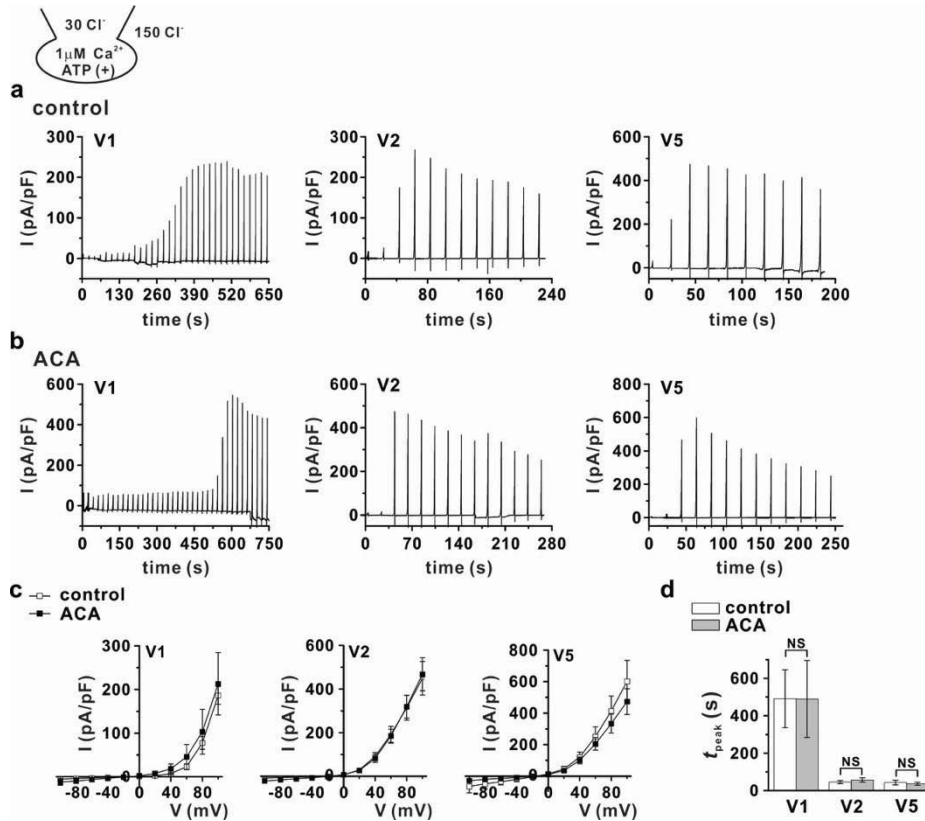
Figure 19. PLA2-independent activation of ANO6 variants 1, 2, and 5

(a) and (b), Representative currents trace of I_{ANO6} generated from the three variants (V1, left panel; V2, middle panel; and V5, right panel) with 1 μM free calcium and 30 mM Cl^- in pipette solution at 37°C, (a) control condition and (b) ACA (20 μM) treated condition, respectively, in ANO6 variant-expressedHEK293T cells. (c), The peak current (I)-voltage (V) relation curve obtained from each variant detected at control condition (open-square) and ACA-treated condition (solid-square). (d), Summary bar graph of t_{peak} of I_{ANO6} of each variant estimated from the trace chart. Data represent the means ± SEM (n=7 for V1 and V2, n = 6 for V5). NS indicates not significant, compared to the control.
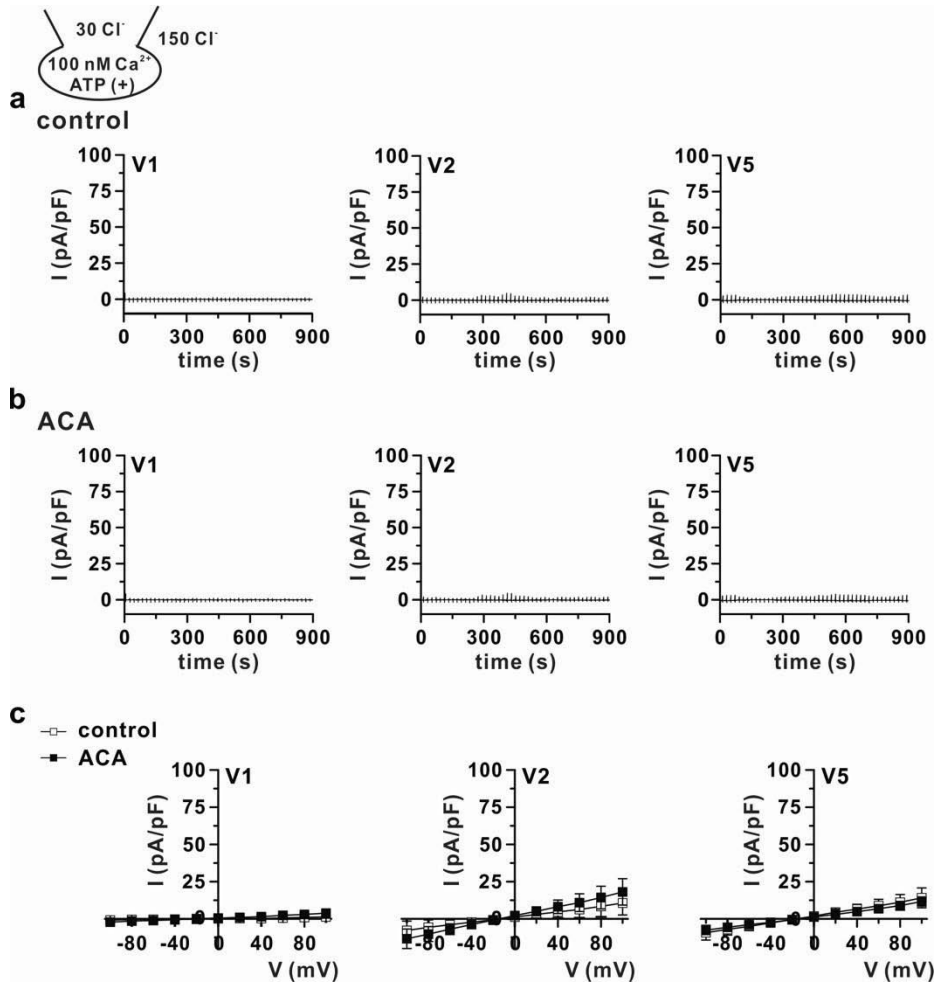
Figure 20. I_{ANO6} of variants with low cytosolic Cl⁻ at 37°C under resting intracellular Ca^{2+}

(a) and (b), Representative trace of the I_{ANO6} of V1 (left-panel), V2 (middle-panel), and V5 (right-panel) with 100 nM free calcium and 30 mM Cl⁻ in pipette solution at 37°C, (a) control condition and (b) ACA (20 μM) treated condition, respectively. (c), Corresponding current (I)–voltage (V) relationship curve obtained from each variant detected at control condition (open-square) and ACA-treated condition (solid-square). Data represent the means ± SEM (n=4 for V1, V2, and V5).
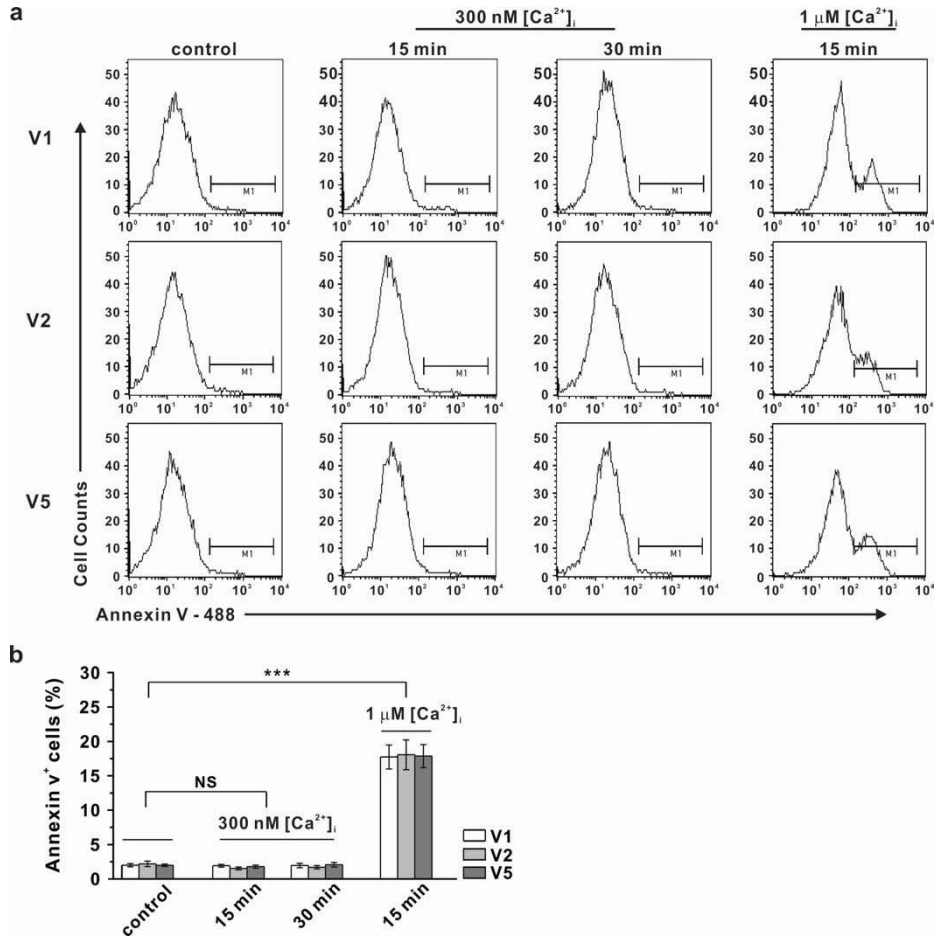
Figure 21. Phosphatidylserine scramblase activity of ANO6 variants V1, V2, and V5 with different $[Ca^{2+}]_i$ at 37°C

(a), Histogram of Annexin V binding, reflecting phosphatidylserine exposure, in ANO6 variants-transfected HEK293T cells. Cells were treated with an appropriate concentration of ionomycin to maintain the intracellular Ca^{2+} concentrations at 300 nM for 15 min and 30 min, and 1 μM for 30 min at 37°C (V1, upper panel; V2, middle panel; and V5, lower panel). (b), Summary bar graph of the response of Annexin V-positive cells [%, percentage of total cell counts (M1)] to ionomycin treatment for each variant. Data are presented as means ± SEM (n=5–6). *** $P < 0.001$ compared to the control, analysed by one-way ANOVA with Tukey's tests.

Discussion

ANO6(TMEM16F) is expressed in various tissues and cell types[25,52]. Nevertheless, the physiological roles of ANO6 have been identified in only limited types of cells such as immunocytes, platelets, and osteoblasts[9,13-15], all of which are thought to be related to its PS scramblase activity[17,53,54]. Conversely, owing to its low calcium channel sensitivity, the potential of ANO6 to function as an ion channel in physiological conditions remains controversial. The present results, instead, provide evidence that a physiologically sustainable increase of submicromolar $[Ca^{2+}]_i$ could activate ANO6 variants over 37°C. In addition, $I_{ANO6}$was detected without significant induction of the scramblase activities of ANO6variants at submicromolar $[Ca^{2+}]_i$ at 37°C.

 In this study, the results revealed that physiological temperature could dramatically lower the $[Ca^{2+}]_i$ required for I_{ANO6} activation, contrary to the exponentially higher values that reported before[23,24], with V2 and V5 being activated even with 300 nM $[Ca^{2+}]_i$ at 37°C. Moreover, temperature increase to 42°C further increased the calcium sensitivity of ANO6, such that V1 could be activated by 300 nM $[Ca^{2+}]_i$ as well. At 42°C, all variants could slightly be activated even with resting Ca^{2+} concentrations of 100 nM in ANO6 – overexpressing HEK293T cells. However, no ANO6 variants showed activation in $[Ca^{2+}]_i$ free conditions even at high temperature (42°C).

My findings also revealed the reversible temperature-dependence of I_{ANO6}. This indicated that the changes in the threshold $[Ca^{2+}]_i$ were not due to unspecific leakiness of the patch clamp conditions. Furthermore, the I_{ANO6} was almost completely recovered and rapidly activated at the second 37°C condition (Fig. 10), suggesting that ANO6 might contribute to a lasting signal response to temperature changes when combined with calcium signaling.

ANO6 activation requires at least tens of seconds for the detectable development of I_{ANO6} and several minutes for steady-state activation even with a relatively high $[Ca^{2+}]_i$[22-24]. However, a recent comparison of the half-activation times of ANO6 variants with 20 μM $[Ca^{2+}]_i$ revealed differential latency times of 3 min for V1 and V5, and >1 min for V2[25]. Thus, to investigate the relationship between temperature and t_{peak}, I compared the change in t_{peak} with the temperature change after fixing $[Ca^{2+}]_i$ at 3 μM in the cells. In particular, the t_{peak} of I_{ANO6} was shortened by about 50 % in the three variants at 37°C. Although the acceleration of t_{peak} was statistically significant, it should be noted that I_{ANO6} activation still required tens of seconds (V2 and V5) or several minutes (> 6 min, V1) at the physiological temperature. However, with respect to peak current amplitudes, even at 37°C, there was no meaningful change in the peak outward currents produced by all three isoforms at 3 μM $[Ca^{2+}]_i$. The delta amplitude of I_{ANO6}

detected between 27°C and 37°C only increased by about 2-fold compared to those detected at room temperature in V2 and V5, whereas V1 showed the same level of activation currents between room temperature (27°C) and 37°C.

However, this result differs from reports on ANO1, which was verified as a heat sensor. In response to temperature change, ANO1 showed increased activated current densities, with a Q_{10} (the 10°C temperature coefficient) value of approximately 19.4, and an increase in $[Ca^{2+}]_i$ lowered the temperature threshold for activating ANO1[5]. Nevertheless, the shortened t_{peak} as well as sub-micromolar $[Ca^{2+}]_i$ threshold in ANO6 variants at physiological temperature (37°C-42°C) are plausible conditions in specific physiological contexts such as under G protein-coupled receptor stimulations for numerous Ca^{2+}-sensitive processes[55], implying the likely electrical roles of ANO6 under physiological conditions.

The abolishment of the latency period for ANO6 activation after membrane excision was briefly described in previous study[24], and was confirmed here for all three functional variants of ANO6. Additionally, different to whole-cell patch, I_{ANO6} was not activated by sub-micromolar $[Ca^{2+}]_i$ in inside-out patch at 37°C. Although the size of I_{ANO6} with 3 μM was increased at 37°C, such changes might reflect the natural thermodynamic energy state of the temperature increase rather than the notable physiological

temperature sensitivity. The dramatic difference in the activation kinetics between I_{ANO6} in whole-cell and inside-out patch clamp suggested that unknown cytosolic factor(s) potently inhibit the activation of ANO6, even with a high $[Ca^{2+}]_i$ combined with the physiological temperature. The candidate intrinsic factors include ATP, phosphorylation states of signaling molecules, cytoskeleton- or calmodulin-dependent signals, and alterations in membrane phospholipids, among others. PLA2 is reported to activate ANO6 only in low cytosolic chloride condition[50,51]. However, in my study, I conclude that the temperature-dependent calcium sensitivity and acceleration of ANO6 variants activation were not due to PLA2 both in symmetrical and low cytosolic chloride conditions (Fig. 17-20). In the first part of study, the negatively regulatory effects of actin cytoskeleton and intracellular ATP were determined. However, more studies are needed to clarify the relationship between temperature changes and actin cytoskeleton rearrangement.

The results of Scudieriet al. (2015)[25] and this study indicate that the Ca^{2+} sensitivity and t_{peak} differ among ANO6 variants. Generally, V2 and V5 are more sensitive to $[Ca^{2+}]_i$ and exhibit relatively faster t_{peak} than V1 at all temperature ranges (Fig. 9 and Fig. 11). Although, more evidence is required to prove this phenomenon, it might be caused by the structural difference between ANO6 variants that underlie their distinguishable biophysical properties,

including the Ca^{2+} sensitivity and t_{peak}. However, in excised patch clamp conditions, the difference in Ca^{2+} sensitivity and t_{peak} between each variant disappears (Fig. 16).

The altered domain structures in the N- and C-termini of the variants have been schematically compared, as shown in Fig. 1a. According to the sequence database, V2 contains only 5 amino acids in contrast to the 23 amino acids in V1 at the initial part of the N-terminus, whereas V5 has an additional 21 amino acids inserted following the first 23 amino acids of V1. Notably, the segment at the first 23 amino acids contains a stretch of eight consecutive acidic amino acid residues (EEEEDDDD). A similar case can be observed in the mammalian Na+/H+ exchanger isoform 1(NHE1), which has seven consecutive acidic residues in the distal region of the cytosolic tail[57]. This site is critical for the maintenance of NHE1 activity and calmodulin binding. Thus, V2 and V5 may be weaker or less affected by the specific regulatory factor than V1. In many cases, as with NHE1, consecutive negative acidic amino acids are often used to regulate the activity of ion channels in the cytoplasm. Therefore, it is necessary to identify the role of this domain in future studies through mutation analyses. As a whole, these findings suggest that the cytosolic initial amino acids of the N-terminus might play an important role for sensing Ca^{2+} and determining the delayed time for activation.

Nevertheless, the exact mechanism of ANO6 activation and the reason for the observed delayed activation remain unknown.

The equal or even more commonly recognized role of ANO6 as a membrane phospholipid scramblase than as an anion channel is consistent with the recognition that some albeit few ion channel proteins show enzymatic functions along with electricalactivity[53]. A recent elaborate study demonstrated that the ion transport through ANO6 constitutes a leak current associated with lipid transport via scramblase activity, which shares the same pathways with ions and phospholipids with 200 μM cytosolic calcium[58]. In contrast, the higher Ca^{2+} sensitivity of I_{ANO6} than the ionomycin dose-dependent PS exposure at 37°C might suggest that that scramblase and channel activities could be separately induced *in vivo*, further supporting the physiological function of ANO6 as an ion channel. However, it should be considered that the PS exposure levels detected in the fluorescence-activated cell sorting (FACS) analysis reflect not only the scramblase but also the intrinsic flippase activity reversing the PS to the inner leaflet. In this respect, the relatively low levels of scramblase activity detected with submicromolar $[Ca^{2+}]_i$ might have been compensated in the current assay system. In contrast, the ionic flow through ANO6 would be more sensitively detected if only the voltage gradient exists.

In summary, I have provided the first demonstration that the

ANO6 isoforms V2 and V5 can be activated within a submicromolar range of cytosolic free calcium at 37°C and that V1 can be activated by 1 μM $[Ca^{2+}]_i$ with a short t_{peak}. Moreover, further increase of the temperature to 42°C, which lowered $[Ca^{2+}]_i$ for activation, could activate all ANO6 variants even with 100 nM $[Ca^{2+}]_i$. This temperature-dependent calcium sensitivity and kinetics of t_{peak} among ANO6 variants require additional detailed study to fully understand the precise mechanisms. Furthermore, ANO6 ion currents were activated by low calcium (300 nM), whereas phospholipid scrambling activity was not detected under these conditions. Thus, the present results provide an experimental foundation for the functional exploration of ANO6 as an ion channel. Further quantitative analysis of variant type expression would be necessary for elucidating their physiological roles in the different tissues expressing ANO6.

REFERENCES

1. Milenkovic VM, Brockmann M, Stohr H, Weber BH & Strauss O. Evolution and functional divergence of the anoctamin family of membrane proteins. *BMC Evol Biol* **10**, 319 (2010).

2. Hwang SJ, Blair PJ, Britton FC, O'Driscoll KE, Hennig G, Bayguinov YR, Rock JR, Harfe BD, Sanders KM & Ward SM. Expression of anoctamin 1/TMEM16A by interstitial cells of Cajal is fundamental for slow wave activity in gastrointestinal muscles. *J Physiol* **587**, 4887-4904 (2009).

3. Ousingsawat J, Martins JR, Schreiber R, Rock JR, Harfe BD & Kunzelmann K. Loss of TMEM16A causes a defect in epithelial Ca2+ -dependent chloride transport. *J Biol Chem* **284**, 28698-28703 (2009).

4. Romanenko VG, Catalan MA, Brown DA, Putzier I, Hartzell HC, Marmorstein AD, Gonzalez-Begne M, Rock JR, Harfe BD & Melvin JE. Tmem16A encodes the Ca^{2+} -activated Cl^- channel in mouse submandibular salivary gland acinar cells. *J Biol Chem* **285**, 12990-13001 (2010).

5. Cho H, Yang YD, Lee J, Lee B, Kim T, Jang Y, Back SK, Na HS, Harfe BD, Wang F, Raouf R, Wood JN & Oh U. The calcium-activated chloride channel anoctamin 1 acts as a heat sensor in nociceptive neurons. *Nat Neurosci* **15**, 1015-1021 (2012).

6. Huang F, Zhang H, Wu M, Yang H, Kudo M, Peters CJ, Woodruff PG, Solberg OD, Donne ML, Huang X, Sheppard D, Fahy JV, Wolters PJ, Hogan BL, Finkbeiner WE, Li M, Jan YN, Jan LY & Rock JR. Calcium-activated chloride channel TMEM16A modulates mucin secretion and airway smooth muscle contraction. *Proc Natl Acad Sci U S A* **109**, 16354-16359 (2012).

7. Stohr H, Heisig JB, Benz PM, Schoberl S, Milenkovic VM, Strauss O, Aartsen WM, Wijnholds J, Weber BH & Schulz HL. TMEM16B, a novel protein with calcium-dependent chloride channel activity, associates with a presynaptic protein complex in photoreceptor terminals. *J Neurosci* **29**, 6809-6818 (2009).

8. Hengl T, Kaneko H, Dauner K, Vocke K, Frings S & Mohrlen F. Molecular components of signal amplification in olfactory sensory cilia. *Proc Natl Acad Sci U S A* **107**, 6052-6057 (2010).

9. Ehlen HW, Chinenkova M, Moser M, Munter HM, Krause Y, Gross S, Brachvogel B, Wuelling M, Kornak U & Vortkamp A. Inactivation of anoctamin-6/Tmem16f, a regulator of phosphatidylserine scrambling in osteoblasts, leads to decreased mineral deposition in skeletal tissues. *J Bone Miner Res* **28**, 246-259 (2013).

10. Harper MT & Poole AW. Chloride channels are necessary

for full platelet phosphatidylserine exposure and procoagulant activity. *Cell Death Dis* **4**, e969 (2013).

11. Kmit A, van Kruchten R, Ousingsawat J, Mattheij NJ, Senden-Gijsbers B, Heemskerk JW, Schreiber R, Bevers EM & Kunzelmann K. Calcium-activated and apoptotic phospholipid scrambling induced by Ano6 can occur independently of Ano6 ion currents. *Cell Death Dis* **4**, e611 (2013).

12. Fujii T, Sakata A, Nishimura S, Eto K & Nagata S. TMEM16F is required for phosphatidylserine exposure and microparticle release in activated mouse platelets. *Proc Natl Acad Sci U S A* **112**, 12800-12805 (2015).

13. Ousingsawat J, Wanitchakool P, Kmit A, Romao AM, Jantarajit W, Schreiber R & Kunzelmann K. Anoctamin 6 mediates effects essential for innate immunity downstream of P2X7 receptors in macrophages. *Nat Commun* **6**, 6245 (2015).

14. Hu Y, Kim JH, He K, Wan Q, Kim J, Flach M, Kirchhausen T, Vortkamp A & Winau F. Scramblase TMEM16F terminates T cell receptor signaling to restrict T cell exhaustion. *J Exp Med* **213**, 2759-2772 (2016).

15. Mattheij NJ, Braun A, van Kruchten R, Castoldi E, Pircher J, Baaten CC, Wulling M, Kuijpers MJ, Kohler R, Poole AW, Schreiber R, Vortkamp A, Collins PW, Nieswandt B,

Kunzelmann K, Cosemans JM & Heemskerk JW. Survival protein anoctamin-6 controls multiple platelet responses including phospholipid scrambling, swelling, and protein cleavage. *FASEB J* **30**, 727-737 (2016).

16. Zaitseva E, Zaitsev E, Melikov K, Arakelyan A, Marin M, Villasmil R, Margolis LB, Melikyan GB & Chernomordik LV. Fusion Stage of HIV-1 Entry Depends on Virus-Induced Cell Surface Exposure of Phosphatidylserine. *Cell Host Microbe* **22**, 99-110 e117 (2017).

17. Suzuki J, Umeda M, Sims PJ & Nagata S. Calcium-dependent phospholipid scrambling by TMEM16F. *Nature* **468**, 834-838 (2010).

18. Castoldi E, Collins PW, Williamson PL & Bevers EM. Compound heterozygosity for 2 novel TMEM16F mutations in a patient with Scott syndrome. *Blood* **117**, 4399-4400 (2011).

19. Martins JR, Faria D, Kongsuphol P, Reisch B, Schreiber R & Kunzelmann K. Anoctamin 6 is an essential component of the outwardly rectifying chloride channel. *Proc Natl Acad Sci U S A* **108**, 18168-18172 (2011).

20. Simoes F, Ousingsawat J, Wanitchakool P, Fonseca A, Cabrita I, Benedetto R, Schreiber R & Kunzelmann K. CFTR supports cell death through ROS-dependent activation of TMEM16F (anoctamin 6). *Pflugers Arch* **470**, 305-314

(2017).

21. Yang H, Kim A, David T, Palmer D, Jin T, Tien J, Huang F, Cheng T, Coughlin SR, Jan YN & Jan LY. TMEM16F forms a Ca^{2+}-activated cation channel required for lipid scrambling in platelets during blood coagulation. *Cell* **151**, 111-122 (2012).

22. Grubb S, Poulsen KA, Juul CA, Kyed T, Klausen TK, Larsen EH & Hoffmann EK. TMEM16F (Anoctamin 6), an anion channel of delayed Ca^{2+} activation. *J Gen Physiol* **141**, 585-600 (2013)

23. Shimizu T, Iehara T, Sato K, Fujii T, Sakai H & Okada Y. TMEM16F is a component of a Ca^{2+}-activated Cl^- channel but not a volume-sensitive outwardly rectifying Cl^- channel. *Am J Physiol Cell Physiol* **304**, C748-759 (2013).

24. Kim HJ, Jun I, Yoon JS, Jung J, Kim YK, Kim WK, Kim BJ, Song J, Kim SJ, Nam JH & Lee MG. Selective serotonin reuptake inhibitors facilitate ANO6 (TMEM16F) current activation and phosphatidylserine exposure. *Pflugers Arch* **467**, 2243-2256 (2015).

25. Scudieri P, Caci E, Venturini A, Sondo E, Pianigiani G, Marchetti C, Ravazzolo R, Pagani F & Galietta LJ. Ion channel and lipid scramblase activity associated with expression of TMEM16F/ANO6 isoforms. *J Physiol* **593**, 3829-3848 (2015).

26. Yang YD, Cho H, Koo JY, Tak MH, Cho Y, Shim WS, Park SP, Lee J, Lee B, Kim BM, Raouf R, Shin YK & Oh U. TMEM16A confers receptor-activated calcium-dependent chloride conductance. *Nature* **455**, 1210-1215 (2008).

27. Xiao Q, Yu K, Perez-Cornejo P, Cui Y, Arreola J & Hartzell HC. Voltage- and calcium-dependent gating of TMEM16A / Ano1 chloride channels are physically coupled by the first intracellular loop. *Proc Natl Acad Sci U S A* **108**, 8891-8896 (2011).

28. Yu K, Whitlock JM, Lee K, Ortlund EA, Cui YY & Hartzell HC. Identification of a lipid scrambling domain in ANO6 / TMEM16F. *Elife* **4**, e06901 (2015).

29. Gee HY, Jun I, Braun DA, Lawson JA, Halbritter J, Shril S, Nelson CP, Tan W, Stein D, Wassner AJ, Ferguson MA, Gucev Z, Sayer JA, Milosevic D, Baum M, Tasic V, Lee MG & Hildebrandt F. Mutations in SLC26A1 Cause Nephrolithiasis. *Am J Hum Genet* **98**, 1228-1234 (2016).

30. Jun I, Lee JS, Lee JH, Lee CS, Choi SI, Gee HY, Lee MG & Kim EK. Adult-Onset Vitelliform Macular Dystrophy caused by BEST1 p.Ile38Ser Mutation is a Mild Form of Best Vitelliform Macular Dystrophy. *Sci Rep* **7**, 9146 (2017)

31. Caputo A, Caci E, Ferrera L, Pedemonte N, Barsanti C, Sondo E, Pfeffer U, Ravazzolo R, Zegarra-Moran O, Galietta LJ. TMEM16A, a membrane protein associated with calcium-

dependent chloride channel activity, *Science* **322**, 590–594 (2008).

32. Pifferi S, Dibattista M, Menini A. TMEM16B induces chloride currents activated by calcium in mammalian cells, *Pflugers Arch* **458**, 1023–1038 (2009).

33. Ye W, Han TW, Nassar LM, Zubia M, Jan YN, Jan LY. Phosphatidylinositol-(4, 5)-bisphosphate regulates calcium gating of small-conductance cation channel TMEM16F. *Proc Natl Acad Sci U S A* **115**, E1667–E1674 (2018).

34. Martinac, B. The ion channels to cytoskeleton connection as potential mechanism of mechanosensitivity. *Biochim Biophys Acta* **1838**, 682–691 (2014).

35. Ohshiro J, Yamamura H, Suzuki Y, Imaizumi Y. Modulation of TMEM16A-channel activity as Ca^{2+} activated Cl^{-} conductance via the interaction with actin cytoskeleton in murine portal vein. *J Pharmacol Sci* **125**, 107–111 (2014).

36. Clark R. & Proks P. ATP-sensitive potassium channels in health and disease. *Adv Exp Med Biol* **654**, 165–192 (2010).

37. Rosenhouse-Dantsker A, Mehta D, Levitan I. Regulation of ion channels by membrane lipids. *Compr Physiol* **2**, 31–68 (2012).

38. Goddette DW & Frieden C. Actin polymerization. The mechanism of action of cytochalasin D. *J Biol Chem* **261**, 15974–15980 (1986)

39. Khurana S. Role of actin cytoskeleton in regulation of ion transport: examples from epithelial cells. *J Membr Biol* **178**, 73–87 (2000).

40. Carlier MF, Valentin-Ranc C, Combeau C, Fievez S, Pantoloni D. Actin polymerization: regulation by divalent metal ion and nucleotide binding, ATP hydrolysis and binding of myosin. *Adv Exp Med Biol* **358**, 71–81 (1994).

41. Korn ED, Carlier MF, Pantaloni D. Actin polymerization and ATP hydrolysis. *Science* **238**, 638–644 (1987).

42. Zhang L, Mao YS, Janmey PA, ß Yin HL. Phosphatidylinositol 4, 5 bisphosphate and the actin cytoskeleton. *Subcell Biochem* **59**, 177–215 (2012).

43. Spiering D & Hodgson L. Dynamics of the Rho-family small GTPases in actin regulation and motility. *Cell Adh Migr* **5**, 170–180 (2011).

44. Kunzelmann K. Ion channels in regulated cell death. *Cell Mol Life Sci* **73**, 2387–2403 (2016).

45. Fujii T, Sakata A, Nishimura S, Eto K, Nagata S. TMEM16F is required for phosphatidylserine exposure and microparticle release in activated mouse platelets. *Proc Natl Acad Sci U S A* **112**, 12800–12805 (2015).

46. Kirov A, Al-Hashimi H, Solomon P, Mazur C, Thorpe PE, Sims PJ, Tarantini F, Kumar TK, Prudovsky I. Phosphatidylserine externalization and membrane blebbing

are involved in the nonclassical export of FGF1. *J Cell Biochem* **113**, 956–966 (2012).

47. Fackler OT & Grosse R. Cell motility through plasma membrane blebbing. *J Cell Biol* **181**, 879–884 (2008).

48. Yarotskyy V & Dirksen RT. Temperature and RyR1 regulate the activation rate of store-operated Ca^{2+} entry current in myotubes. *Biophys J* **103**, 202–211 (2012).

49. Yang F & Zheng J. High temperature sensitivity is intrinsic to voltage-gated potassium channels. *Elife* **3**, e03255 (2014).

50. Schreiber R, Ousingsawat J, Wanitchakool P, Sirianant L, Benedetto R, Reiss K, Kunzelmann K. Regulation of TMEM16A/ANO1 and TMEM16F/ANO6 ion currents and phospholipid scrambling by Ca^{2+} and plasma membrane lipid. *J Physiol* **596**, 217–229 (2018).

51. Sirianant L, Ousingsawat J, Wanitchakool P, Schreiber R & Kunzelmann K. Cellular volume regulation by anoctamin 6: Ca^{2+}, phospholipase A2 and osmosensing. *Pflugers Arch* **468**, 335–349 (2016).

52. Liu G, Chen H, Borst O, Gawaz M, Vortkamp A, Schreiber R, Kunzelmann K & Lang F. Involvement of Ca^{2+} activated Cl^- channel Ano6 in platelet activation and apoptosis. *Cell Physiol Biochem* **37**, 1934–1944 (2015).

53. Malvezzi M, Chalat M, Janjusevic R, Picollo A, Terashima

H, Menon AK & Accardi A. Ca^{2+}-dependent phospholipid scrambling by a reconstituted TMEM16 ion channel. *Nat Commun* **4**, 2367 (2013).

54. Gyobu S, Ishihara K, Suzuki J, Segawa K & Nagata S. Characterization of the scrambling domain of the TMEM16 family. *Proc Natl Acad Sci U S A* **114**, 6274-6279 (2017).

55. Berridge MJ, Lipp P & Bootman MD. The versatility and universality of calcium signalling. *Nat Rev Mol Cell Biol* **1**, 11-21 (2000).

56. Schreiber R, Ousingsawat J, Wanitchakool P, Sirianant L, Benedetto R, Reiss K & Kunzelmann K. Regulation of TMEM16A/ANO1 and TMEM16F/ANO6 ion currents and phospholipid scrambling by Ca^{2+} and plasma membrane lipid. *J Physiol* **596**, 217-229 (2018).

57. Li X, Ding J, Liu Y, Brix BJ & Fliegel L. Functional analysis of acidic amino acids in the cytosolic tail of the Na^{+}/H^{+} exchanger. *Biochemistry* **43**, 16477-16486 (2004).

58. Yu K, Whitlock JM, Lee K, Ortlund EA, Cui YY & Hartzell HC. Identification of a lipid scrambling domain in ANO6/TMEM16F. *Elife* **4**, e06901 (2015).

국문초록

Anoctamin 6 (ANO6, TMEM16F)은 칼슘의존성 염소이온통로 (CaCC)와 phospholipid scramblase 기능을 함께 갖고 있는 세포막 단백질이다. ANO6은 다른 CaCC (예: ANO1)와 비교할 때, 매우 높은 세포 내 칼슘 증가 상태에서도 훨씬 느리게 활성화되기 때문에 생리적으로 이온통로 기능이 유의미한지에 대한 논란이 많다. 이처럼 느린 활성화에 대해 1) 세포내 ATP의존적인 액틴섬유 세포골격의 변화, 2) 온도 조건 (실온 또는 체온)의 차이가 원인일 수 있다는 가설을 설정하고, 이를 팻취클램프 기법으로 증명하고자 했다.

 ANO6 접합변이형 중 제1형 (V1) 과발현 세포에서 whole-cell 팻취클램프로 전류를 기록했다. 세포내용액에 ATP가 포함되면 ANO6 전류 활성화가 억제됐다. 액틴섬유 저해제인 cytochalasin D를 처리 후 전류를 기록하면, ANO6 전류 활성화가 빨라졌고, 액틴섬유 강화제인 phalloidin과 jasplakinolide 처리하면 ANO6 전류는 훨씬 느리게 활성화됐다. 세포골격단백이 파괴될 것으로 예상되는 inside-out 팻취클램프 조건에서, ANO6은 세포막 안쪽 칼슘 증가에 따라 즉각 활성화됐다. 이러한 결과는 세포의 액틴섬유의 유지 정도가 ANO6의 이온통로 활성화를 억제할 수 있음을 시사한다.

 ANO6의 네 가지 접합변이형들 (V1, V2, V3 와 V5) 중 V3는 세포막에 발현되지 않았고, 나머지 변이형들은 모두 낮은 칼슘 민감성과 느린 활성화를 보였다. 실험 용액 온도를 실온 (25도)에서 37도로 올리면, 모든 접합변이형들의 칼슘 민감도가 증가하고, 전류

활성화가 빨라졌다. 하지만 ANO6의 다른 기능인 scramblase 활성은 37도 조건에서도 여전히 칼슘 민감도가 낮았다. 흥미롭게도, inside-out patch clamp 조건에서는 온도를 올리더라도 ANO6 전류 활성화의 칼슘민감도는 유의한 변화가 없었다.

 종합해보면, 체온 수준 또는 그 이상의 온도 조건 및 액틴섬유의 중합이 저해되는 조건에서 ANO6은 기존 보고들보다 낮은 생리적 범위의 칼슘농도에서도 활성화되면서, 이온통로로서 생리학적 기능을 할 것으로 추정된다.

주요어: 세포내골격단백질, 칼슘 의존성 염소이온통로,
접합변이형, 온도, 칼슘 민감성